Pharmacological targeting of STK19 inhibits oncogenic NRAS driven melanomagenesis

Chengqian Yin[1, 12], Bo Zhu[1, 12], Ting Zhang[2, 12], Tongzheng Liu[3, 12], Shuyang Chen[1], Yu Liu[4], Xin Li[1], Xiao Miao[5], Shanshan Li[1], Xia Mi[1], Jie Zhang[6], Li Li[2], Guo Wei[7], Zhi-xiang Xu[8], Xiumei Gao[9], Canhua Huang[4], Zhi Wei[6], Colin R. Goding[10], Peng Wang[11, *], Xianming Deng[2, *], Rutao Cui[1, 13, *]

[1]Department of Pharmacology and Experimental Therapeutics, Boston University School of Medicine, Boston, MA 02118, USA

[2]State Key Laboratory of Cellular Stress Biology, Innovation Center for Cell Signaling Network, School of Life Sciences, Xiamen University, Xiamen, Fujian 361102, China

[3]Jinan University Institute of Tumor Pharmacology, Guangzhou, Guangdong 510632, China

[4]State Key Laboratory of Biotherapy and Cancer Center, West China Hospital, Sichuan University and National Collaborative Innovation Center, Chengdu, Sichuan 610041, China

[5]Innovation Research Institute of traditional Chinese Medicine, Shanghai University of Traditional Chinese Medicine, Shanghai 200000, China

[6]Department of Computer Science, New Jersey Institute of Technology, Newark, NJ 07102, USA

[7]The Broad Institute of the Massachusetts Institute of Technology and Harvard University, Cambridge, MA 02142, USA

[8]Division of Hematology/Oncology, Department of Medicine, University of Alabama at Birmingham School of Medicine, Birmingham, AL 35233, USA

[9]Tianjin State Key Laboratory of Modern Chinese Medicine, Tianjin University of Traditional Chinese Medicine, Tianjin 300193, China

[10]Ludwig Institute for Cancer Research, University of Oxford, Headington, Oxford, OX3 7DQ, UK

[11]Department of Integrative Oncology, Fudan University Shanghai Cancer Center, Shanghai 200032, China

[12]These authors contributed equally.

[13]Lead Contact

[*]Correspondence: rutaocui@bu.edu (R.C.), xmdeng@xmu.edu.cn (X.D.), or wangp413@163.com (P.W.)

SUMMARY

Activating mutations in NRAS account for 20-30% of melanoma, but despite decades of research and in contrast to BRAF, no effective anti-NRAS therapies have been forthcoming. Here we identify a previously uncharacterized serine/threonine kinase STK19 as a novel NRAS activator. STK19 phosphorylates NRAS to enhance its binding to its downstream effectors and promotes oncogenic NRAS-mediated melanocyte malignant transformation. A recurrent D89N substitution in STK19 whose alterations were identified in 25% of human melanomas represents a gain-of-function mutation that interacts better with NRAS to enhance melanocyte transformation. $STK19^{D89N}$ knockin leads to skin hyperpigmentation and promotes $NRAS^{Q61R}$-driven melanomagenesis *in vivo*. Finally, we developed ZT-12-037-01 (**1a**) as a specific STK19-targeted inhibitor and showed that it effectively blocks oncogenic NRAS-driven melanocyte malignant transformation and melanoma growth *in vitro* and *in vivo*. Together, our findings provide a new and viable therapeutic strategy for melanomas harboring NRAS mutations.

INTRODUCTION

RAS proteins are small membrane-bound guanine nucleotide-binding GTPases, acting as molecular switches by converting between GDP-bound inactive state and GTP-bound active state (Bos, 1989; Downward, 2003; Milburn et al., 1990; Pylayeva-Gupta et al., 2011). They play a central role in the regulation of cell proliferation, differentiation and survival by activating different downstream signaling pathways including RAF-MEK-ERK and PI3K-AKT pathways (Downward, 2003; Lavoie and Therrien, 2015; Mendoza et al., 2011; Samatar and Poulikakos, 2014). The RAS family has three major isoforms, KRAS, HRAS and NRAS (Barbacid, 1987; Malumbres and Barbacid, 2003) that share 92-98% sequence identity in the amino-terminal 1-165 residues but substantially diverge in the carboxy-terminal 23-24 residues of hypervariable region (HVR) (Krengel et al., 1990; Prior et al., 2012). Oncogenic mutations of RAS family members are commonly found in 20% to 30% of all human tumors (Prior et al., 2012; Stephen et al., 2014). Despite the highly conserved sequence similarity, the three major RAS isoforms exhibit distinct preferences in coupling to particular cancer types (Pylayeva-Gupta et al., 2011; Stephen et al., 2014). For instance, oncogenic mutations of KRAS are most identified in pancreatic ductal adenocarcinomas (PDAC) and colorectal adenocarcinomas (CRC) (Cox et al., 2014), HRAS mutations are frequently associated with bladder cancer (Cox et al., 2014; Prior et al., 2012), whereas NRAS mutations occur most frequently in cutaneous melanomas and acute myeloid leukemia (Bacher et al., 2006; Goel et al., 2006; Prior et al., 2012).

The prevailing NRAS mutation in melanoma occurs at position 61, where glutamine is substituted by arginine/lysine/leucine (Q61R/K/L) (Bos, 1989; Hayward et al., 2017; Jakob et al., 2012). This mutation impairs the intrinsic GTP hydrolysis activity and traps NRAS in a constitutive GTP-bound active conformation, which recruits RAF to the inner membrane for dimerization and activation (Marais et al., 1995; Smith et al., 2013). The most frequent mutation of BRAF (approximately 90%) is the substitution

of valine to glutamate at position 600 (Davies et al., 2002). The $BRAF^{V600E}$ mutation increases its kinase activity more than 10.7-fold and stimulates constitutive activation of the downstream MEK-ERK signaling (Davies et al., 2002; Wan et al., 2004; Wellbrock et al., 2004). The oncogenic activation of NRAS and BRAF leads to growth factor-independent proliferation of melanocytes and finally transformation to melanoma (Davies et al., 2002; Ji et al., 2012). Thus, NRAS Q61 mutations and $BRAF^{V600E}$ mutation are key drivers of melanomagenesis and important therapeutic targets. Unlike the well-defined BRAF inhibitors, the development of direct NRAS-selective inhibitors has been unsuccessful in the past decades (Cox et al., 2014).

Oncogenic activity of RAS depends on its localization at the inner face of the plasma membrane and its subsequent association with major effectors for downstream signal transduction, which are modulated by RAS posttranslational modifications including prenylation, palmitoylation and phosphorylation (Ahearn et al., 2011; Barcelo et al., 2013; Berndt et al., 2011; Chiu et al., 2002; Jackson et al., 1990). Prenylation at the CAAX box cysteine and addition of a palmitic moiety to a second cysteine residue in the C-terminal hypervariable region (HVR) result in hydrophobic anchors to localize RAS to the plasma membrane (Buss and Sefton, 1986; Casey et al., 1989; Wright and Philips, 2006). RAS phosphorylation at different sites also distinctly regulates RAS activity. Phosphorylation at tyrosine 32 by SRC promotes the intrinsic GTPase activity of RAS to downregulate RAS signaling pathway (Bunda et al., 2014), whereas phosphorylation at tyrosine 137 by ABL allosterically enhances the binding of RAS to RAF (Ting et al., 2015). Phosphorylation at serine 181 of oncogenic KRAS is required for tumor growth and apoptosis inhibition (Barcelo et al., 2014). Therefore, targeting the regulators of RAS modification may provide a novel perspective to develop anti-RAS therapies for cancer treatment.

The human STK19 gene (also named as G11 or RP1) localizes in the class III region of the major histocompatibility complex (MHC) (Sargent et al., 1994). STK19 protein consists of 368 amino acids and

two major functional domains: the regulatory domain (1-110 aa) and the catalytic kinase domain (111-368 aa) (Gomez-Escobar et al., 1998). STK19 was originally reported to phosphorylate α-casein at serine/threonine residues and histones at serine residues (Gomez-Escobar et al., 1998). Recently, it has been reported to involve in transcription-related DNA damage response (Boeing et al., 2016). However, the role of STK19 in cancer initiation and development is poorly appreciated. Importantly, STK19 harbors significant somatic hot spot mutations in 5% of melanoma (Hodis et al., 2012) and 10% of skin basal cell carcinoma (Bonilla et al., 2016) respectively, and is listed among the top melanoma driver genes (Lawrence et al., 2014). This strong genetic evidence implies an important, but uncharacterised role of STK19 in melanocyte malignant transformation and melanoma progression.

In this study, we set out to use melanoma as a model to identify novel strategies for targeting oncogenic RAS signaling by identifying kinases that regulate NRAS activity and leading to the discovery of STK19. We demonstrated that STK19 phosphorylates NRAS at serine 89, and consequently enhanced binding between NRAS and its effectors and activated NRAS downstream signaling pathways to induce melanocyte malignant transformation. We also showed that the frequent D89N substitution detected in melanoma patients represents a gain-of-function mutation in STK19 that in knock-in mice causes skin hyperpigmentation and promotes oncogenic NRAS-driven melanomagenesis. By developing a specific and novel STK19-targeted inhibitor, ZT-12-037-01 (**1a**), we were able to effectively blockade oncogenic NRAS-driven melanocyte malignant transformation and melanoma growth. Our results reveal how targeting STK19 may provide an effective therapeutic strategy for NRAS mutant melanomas.

RESULTS

STK19 is a critical regulator of NRAS function

Activation of NRAS signaling depends on its association with effector proteins, such as RAF and PI3K, that contain a common RAS-binding domain (RBD) (Pylayeva-Gupta et al., 2011). Disrupting the NRAS-RBD protein interaction would represent an effective therapy in NRAS mutant melanoma. To achieve this objective, we screened for kinases that could regulate the activity of $NRAS^{Q61R}$, the most prevalent NRAS mutation found in melanoma (Jakob et al., 2012). We therefore established HEK293FT cells expressing HA-tagged $NRAS^{Q61R}$ and screened a primary human kinome siRNA library using a modified active NRAS chemiluminescence assay as a readout. Specifically, HA-$NRAS^{Q61R}$ from siRNA-transfected cells was captured using a GST-CRAF-RBD fusion protein on glutathione-coated plates, and detected with an anti-HA tag antibody conjugated with horseradish peroxidase for luminescence quantification (**Figure 1A**). We initially identified 12 kinases whose knockdown led to more than 50% inhibition of $NRAS^{Q61R}$ activity, and six kinases whose knockdown led to at least two-fold upregulation of $NRAS^{Q61R}$ activity (**Figure 1B**). Among these genes, EGFR, SYK and SRC are well-known regulators of NRAS functions (Bunda et al., 2014; Downward, 2003; Kawakami et al., 2003). However, of all the hits, STK19 was one of the candidates whose knockdown caused the highest inhibition on NRAS activity (35.1% of control group) (**Figure 1B**). To identify the status of STK19 in human melanomas, we investigated STK19 alteration in the TCGA melanoma cohort (PanCancer Atlas) and found STK19 to be altered in 91 of 363 (25.07%) sequenced skin cutaneous melanoma cases (**Figure 1C**). This is consistent with the analysis of large-scale melanoma exome data that discovered STK19 as one of six novel melanoma genes (PPP6C, RAC1, SNX31, TACC1, STK19, and ARID2) with a statistically significant functional mutation burden (Hodis et al., 2012). As such, STK19 has been listed as an oncogenic candidate among the Broad Institute melanoma driver genes (Lawrence et al., 2014). Analysis of STK19 alteration in melanomas collected in different cBioPortal for Cancer Genomics databases further confirmed this discovery (Berger et al., 2012; Hodis et al., 2012; Hugo et al., 2016). However, the function of STK19 is largely uncharacterized,

particularly in melanoma initiation and progression. We found that STK19 alteration was significantly mutually exclusive with BRAF in human melanomas (P=0.002) (**Figure S1A**), consistent with BRAF lying downstream from NRAS activation (Lavoie and Therrien, 2015). Given these observations, we further investigated the potential role of STK19 in regulating NRAS functions in melanomas.

Oncogenic NRAS plays a critical role in melanoma cell growth, which is mediated by its downstream signaling pathways including RAF-MEK-ERK and PI3K-AKT pathways (Ji et al., 2012). To confirm whether STK19 knockdown inhibits NRAS activity, we investigated whether the downstream signaling of NRAS was inhibited after STK19 silencing. Retroviruses encoding empty HA, HA-tagged wild-type NRAS or $NRAS^{Q61R}$ were introduced into human primary melanocytes (HPMs) depleted of STK19. The active-RAS pull-down assay indicated that depletion of STK19 markedly decreased the active fraction of both wild type and oncogenic NRAS, and that consequently signaling downstream from NRAS via the RAF-MEK-ERK and PI3K-AKT pathways was diminished (**Figure 1D**). We also used melanoma cells with different NRAS mutation status to identify the role of STK19 in regulating endogenous NRAS. To this end, STK19 was silenced in A375 and UACC62 cells, both with $BRAF^{V600E}$ and wild-type NRAS, or SK-MEL-2 and WM2032 cells that both express $NRAS^{Q61R}$ and wild-type BRAF (Barretina et al., 2012; Herlyn et al., 1985). Interestingly, inhibition of active NRAS and its downstream effectors (p-MEK, p-ERK1/2, p-AKT) was highly efficient in SK-MEL-2 and WM2032 ($NRAS^{Q61R}$, $BRAF^{WT}$) cells, but the inhibition was much weaker in A375 and UACC62 ($BRAF^{V600E}$, $NRAS^{WT}$) cells (**Figure S1B**). Consistently, depletion of STK19 significantly decreased the growth rate of SK-MEL-2 and WM2032 ($NRAS^{Q61R}$, $BRAF^{WT}$) cells, but had a much smaller effect on the $BRAF^{V600E}$, $NRAS^{WT}$ cells or primary melanocytes (**Figure S1C**). To confirm that inhibition of NRAS signaling was mediated by STK19 knockdown, two new sets of STK19-targeted shRNA were exploited and the resulting depletion of STK19 notably inhibited NRAS activity and its downstream signaling in SK-MEL-2 and WM2032 cells (**Figures**

S1D and S1E). Furthermore, we performed rescue experiments and infected the STK19-depleted melanoma cells with retroviruses encoding empty Flag or Flag-tagged STK19. The ectopic expression of STK19-Flag restored the activation of NRAS signaling (**Figure S1F**), confirming that the inhibition of NRAS signaling using STK19-specific shRNAs was mediated by knockdown of STK19 rather than the off-target effects. Collectively, these results suggest that STK19 has a crucial role in activating oncogenic $NRAS^{Q61R}$ -driven signaling.

To explore the potential role of STK19 in $NRAS^{Q61R}$-driven tumorigenesis, the role of STK19 in melanocyte proliferation and malignant transformation was evaluated using genetically engineered human immortalized melanocytes (hTERT/p53DD/CDK4(R24C)) (Lissanu Deribe et al., 2016) expressing $NRAS^{Q61R}$ together with STK19 silencing. The results indicated that silencing STK19 (**Figure S1G**) substantially inhibited the colony formation capacity of $NRAS^{Q61R}$-transformed melanocytes (**Figure 1E**), as well as their proliferation (**Figure S1H**) and tumor-forming ability in xenografts (**Figures 1F-1H**). These results suggest that STK19 is critical for $NRAS^{Q61R}$-driven melanomagenesis.

STK19 phosphorylates NRAS protein at serine 89

To identify the direct substrates of STK19, cell lysates collected from SK-MEL-2 cells expressing human recombinant Flag-tagged STK19 protein were purified using anti-Flag beads and the interaction factors analyzed by liquid chromatography/tandem mass spectrometry (LC-MS/MS) to identify STK19-interacting proteins (**Figure S2A**). NRAS was identified as one of the most abundant STK19-interacting proteins on the basis of total number of unique peptides (13) (**Figure 2A**). Reciprocal co-immunoprecipitation confirmed that endogenous STK19 strongly interacted with NRAS in SK-MEL-2 and WM2032 cells ($NRAS^{Q61R}$), but bound less well in A375 and UACC62 cells (expressing wild type NRAS) (**Figures S2B and S2C**). The $NRAS^{Q61R}$-STK19 interaction was confirmed by reciprocal co-

immuno-precipitation from HPMs exogenously expressing STK19-Flag and HA-NRAS WT or Q61R mutant (**Figures 2B and 2C**). These results indicate that STK19 directly interacts with NRAS, and especially with $NRAS^{Q61R}$.

To address the significance of the STK19-$NRAS^{Q61R}$ interaction, we asked whether NRAS was an STK19 substrate. Phosphorylated-serine, -threonine and -tyrosine in NRAS were detected in cellular lysates collected from HPMs expressing ectopic STK19 and NRAS (WT or Q61R) after NRAS immunoprecipitation (**Figure 2D**). Strikingly, serine, but not threonine or tyrosine phosphorylation of $NRAS^{Q61R}$ mutant was substantially increased by STK19 expression, and only a marginal increase in phosphorylation of $NRAS^{WT}$ was detected. We also observed robust endogenous NRAS phosphorylation in a panel of melanoma cells expressing $NRAS^{Q61R}$ (**Figure S2D**) whereas phosphorylation of NRAS at serine residues was barely detectable in cells following STK19 silencing (**Figures S2E and S2F**). The upregulation of phosphorylated serine levels in NRAS was also diminished by overexpression of a kinase-dead STK19 K317P mutant (Gomez-Escobar et al., 1998) (**Figures S2G and S2H**). These results suggest that STK19 phosphorylates NRAS at serine residues.

The preferential phosphorylation of $NRAS^{Q61R}$ compared to $NRAS^{WT}$ was also observed using an *in vitro* kinase assay (**Figure S2I**), suggesting that STK19 has a stronger preference towards GTP-loaded active NRAS. To verify this, we further performed an *in vitro* kinase assay using purified NRAS recombinant protein preloaded with GDP, GTP or GTPγS in the presence of recombinant STK19. We found a higher STK19-induced phosphorylation of the GTP- and GTPγS-loaded NRAS than GDP-loaded NRAS (**Figure S2J**). This was confirmed in experiments that showed STK19-induced phosphorylation of different NRAS mutant isoforms was more efficient than that of $NRAS^{WT}$ (**Figure S2K**).

To identify the specific NRAS serine residue(s) phosphorylated by STK19, we performed mass spectrometry after *in vitro* phosphorylation of recombinant $NRAS^{Q61R}$ by purified recombinant STK19

protein. This approach identified phosphorylation of the evolutionarily conserved NRAS serine 89 (S89) (**Figures 2E and 2F**). In agreement with this observation, mutation of S89 to alanine (S89A) abolished phosphorylation of $NRAS^{WT}$ and $NRAS^{Q61R}$ (**Figure 2G**).

To confirm that STK19 upregulates NRAS activity through phosphorylating NRAS protein at S89, HA-$NRAS^{WT}$, HA-$NRAS^{S89A}$, HA-$NRAS^{Q61R}$ or HA-$NRAS^{Q61R/S89A}$ were expressed in HPMs expressing ectopic STK19-Flag. After immunoprecipitation of NRAS WT or mutants, immunoblots were performed to detect interactions between NRAS and its effectors, including BRAF, CRAF and PI3Kα. We found that STK19 overexpression dramatically enhanced the interaction between $NRAS^{Q61R}$ and its effectors, and also stimulated signaling downstream of NRAS as detected by immunoblotting whole cell extracts (**Figure 2H**). No effects of STK19 were observed on a phosphorylation-defective form of NRAS ($NRAS^{S89A}$) or its signaling. By contrast, the introduction of phosphomimetic $NRAS^{Q61R/S89D}$ enhanced NRAS interaction with its effectors and its downstream signaling (**Figure S2L**). These data strongly suggest that STK19-regulated $NRAS^{Q61R}$ activity is largely dependent on the phosphorylation at NRAS S89. Using HPMs expressing $NRAS^{WT}$, $NRAS^{Q61R}$ and $NRAS^{Q61R/S89A}$ mutants alone or together with STK19 (**Figure S2M**) revealed that STK19-stimulated NRAS-driven melanocyte proliferation and malignant transformation were inhibited by the NRAS S89A mutation in assays for colony formation (**Figure 2I**), cell proliferation (**Figure S2N**), and xenograft tumor assays (**Figures 2J-2L**). Moreover, mutation of S89 to phosphomimetic aspartate in the $NRAS^{Q61R}$ mutant (**Figure S2O)** strongly promoted melanocyte colony formation (**Figure S2P**), proliferation (**Figure S2Q**) and tumor formation (**Figures S2R-S2T**). Taken together, our data indicate that STK19-mediated phosphorylation of NRAS at S89 activates oncogenic NRAS-driven melanomagenesis.

STK19 D89N is a recurrent gain-of-function mutation

STK19 has a statistically significant mutation burden in melanoma, and a total of 19 mutations were identified in the TCGA melanoma database as of December of 2017. Strikingly, 8 of them (~42%) were the same mutation (D89N), and most of the other mutations were adjacent to this region (**Figure 3A**), suggesting STK19 D89 is a dominant mutant site in melanoma. These findings are consistent with Hodis et al's exon sequence discovery that STK19 is an important cancer gene with a hot spot mutation pattern in melanoma (Hodis et al., 2012). We have shown that STK19 phosphorylates NRAS to activate its downstream signaling (**Figures 1 and 2**). However, it remained unclear how the $STK19^{D89N}$ might affect NRAS protein modification and activation. We therefore performed an *in vitro* kinase assay to compare the activity of $STK19^{WT}$ and $STK19^{D89N}$ mutant. We found that phosphorylation of purified recombinant NRAS was enhanced by $STK19^{D89N}$ to a higher extent than by $STK19^{WT}$ (**Figure 3B**). Accordingly, compared to $STK19^{WT}$, the $STK19^{D89N}$ mutant co-immunoprecipitated more efficiently with NRAS, enhanced NRAS phosphorylation and activated higher NRAS downstream signaling (**Figures 3C, S3A and S3B**), and also promoted proliferation of SK-MEL-2 and WM2032 melanoma cells (**Figure S3C**). These data suggest that the recurrent $STK19^{D89N}$ mutation represents a gain-of-function mutation that operates by enhancing NRAS signaling.

To identify the role for $STK19^{D89N}$ in driving melanocyte malignant transformation, $STK19^{D89N}$ was expressed in human immortalized primary melanocytes (hTERT/p53DD/CDK4(R24C)) expressing wild type or mutant NRAS with endogenous STK19 silenced (**Figure S3D**) and the resulting cells assayed for colony formation, proliferation and tumor formation. The results revealed that in the presence of oncogenic $NRAS^{Q61R}$, $STK19^{D89N}$ significantly promoted melanocyte colony formation (**Figure 3D**), proliferation (**Figure S3E**) and tumor formation (**Figures 3E-3G**). Collectively these data indicate that $STK19^{D89N}$, a gain-of-function mutation, contributes to melanomagenesis in the presence of activated NRAS.

STK19 D89N induces melanomagenesis in the presence of oncogenic NRAS *in vivo*

To better understand the role of STK19 in melanocytes and melanomagenesis *in vivo*, we generated $STK19^{WT}$ or $STK19^{D89N}$ CRISPR-knockin mice. cDNA encoding human $STK19^{WT}$ or $STK19^{D89N}$ was subcloned into a CRISPR/Cas9-mediated homologous recombination vector targeting the *ROSA26* locus and injected into single-cell embryos of C57BL/6J mice (Chu et al., 2016). The exogenous transcription of the knockin alleles was controlled by using the CAG hybrid promoter. To spatiotemporally control knockin gene expression, a loxP-flanked transcriptional stop element was placed downstream of the CAG promoter (**Figure S4A**). The *ROSA26* locus targeting of $STK19^{WT}$ and $STK19^{D89N}$ allele was confirmed by PCR (**Figure S4B**). Both $STK19^{WT}$ and $STK19^{D89N}$ knockin mice develop normally. The knockin mice with correct insertion were further intercrossed with the Tyr-CreERT2 mouse strain expressing Cre recombinase directed by the melanocyte-specific tyrosinase promoter/enhancer to achieve Tyr-Cre-$STK19^{WT}$ and Tyr-Cre-$STK19^{D89N}$ mice and the expression of $STK19^{WT}$ and $STK19^{D89N}$ protein was confirmed by immunoblotting (**Figure S4C**). Remarkably, the Tyr-Cre-$STK19^{D89N}$ mice, but not the $STK19^{WT}$ mice, exhibited hyperpigmentation of the skin, ears and tail, and the melanin content in skin was significantly increased after tamoxifen induction (**Figures 4A-4E**), similar to the hyperpigmentation observed when oncogenic NRAS is targeted to the melanocyte lineage (Ackermann et al., 2005; Burd et al., 2014b).

To determine whether the overexpression of $STK19^{WT}$ and $STK19^{D89N}$ contributes to melanomagenesis in the presence of oncogenic $NRAS^{Q61R}$, Tyr-Cre-$STK19^{WT}$ or -$STK19^{D89N}$ mice were crossed with loxP/STOP/loxP $NRAS^{Q61R}$ knockin (LSL-$NRAS^{Q61R}$) mice (Ackermann et al., 2005; Burd et al., 2014a) to generate Tyr-Cre-$NRAS^{Q61R}$-$STK19^{WT}$ or Tyr-Cre-$NRAS^{Q61R}$-$STK19^{D89N}$ knockin mice. The effects of $STK19^{WT}$ or $STK19^{D89N}$ knockin in activating NRAS signaling pathways were detected and confirmed

by immunoblot analysis of primary mouse melanocytes derived from the relevant engineered mice. The results obtained using antibodies to detect phosphorylated ERK1/2 and AKT indicated that STK19, and especially the STK19 ^{D89N} mutant, enhanced oncogenic NRAS signaling (**Figure 4F**). By observing melanoma incidence and other skin abnormalities after tamoxifen induction for one year (**Figure S4D**), we found that exogenous expression of STK19^{WT} and STK19^{D89N} accelerated initiation and incidence of melanoma in NRAS^{Q61R} knockin mice (**Figure 4G**). Specifically, melanoma was first diagnosed 295, 211 and 166 days after the tamoxifen injection in Tyr-Cre-NRAS^{Q61R}, Tyr-Cre-NRAS^{Q61R}-STK19^{WT} and Tyr-Cre-NRAS^{Q61R}-STK19^{D89N} knockin mice, respectively. Significantly, melanoma was diagnosed in 78.9% of Tyr-Cre-NRAS^{Q61R}-STK19^{D89N} knockin mice and 47.4% of Tyr-Cre-NRAS^{Q61R}-STK19^{WT} mice (P=0.0269) compared to 11.1% of Tyr-Cre-NRAS^{Q61R} mice (P<0.001 and P=0.0116, respectively). Thus, the STK19^{D89N} mutation increased melanoma incidence 7-fold on the NRAS^{Q61R} background versus NRAS^{Q61R} alone. The melanoma tissues from Tyr-Cre-NRAS^{Q61R}, Tyr-Cre-NRAS^{Q61R}-STK19^{WT}, and Tyr-Cre-NRAS^{Q61R}-STK19^{D89N} mice were also collected for immunoblot analysis to investigate activities of NRAS signaling. The results revealed that STK19^{WT} and especially STK19^{D89N} strongly enhanced signaling downstream from NRAS (**Figure S4E**). These results confirm that STK19, and particularly the STK19^{D89N} mutant, promotes oncogenic NRAS-driven melanomagenesis *in vivo*.

Development of ZT-012-037-1 (1a) as a specific small molecule STK19 inhibitor

Given the pivotal role of NRAS signaling in melanomagenesis and the prominent role of STK19 in NRAS activation, targeting STK19 would represent a potential new therapeutic strategy in melanoma, especially in those with NRAS mutations. Therefore, to identify pharmacological inhibitors of STK19 kinase activity, we screened an in-house library of small molecule compounds based on an optimized biochemical ADP generation assay using recombinant purified human STK19 and NRAS^{Q61R} proteins (**Figure S5A**). The

optimal kinase reaction conditions were chosen through multiple rounds of optimization and validation (**Figures S5B and S5C**). MP-IN-317, also known as UNC0642, a selective G9a and GLP histone lysine methyltransferase inhibitor (Liu et al., 2013), was initially identified as the best hit. We then performed structure-activity relationship (SAR) studies to improve the selectivity and reduce off-target effects towards STK19. After iterative rounds of medicinal chemistry optimization, ZT-12-037-01 (**1a**) was obtained (**Figure 5A**) with similar potent inhibitory activity against STK19 compared to MP-IN-317 with an IC_{50} of 24.04 nM and 30.45 nM respectively (**Figure 5B**), but remarkably decreased inhibitory activity towards the G9a histone lysine methyltransferase with an IC_{50} of 467.4 nM and 7.01 nM (**Figure S5D**). On the other hand, another G9a/GLP specific inhibitor A-366 with different chemical scaffold (Sweis et al., 2014), showed little inhibitory potential toward STK19 (**Figure S5E**). Additionally, **1a** was determined to have extremely high kinase selectivity using KINOMEscan (**Table S1**), which profiled the inhibitor at a concentration of 1 μM against a panel of 468 diverse kinases using an *in vitro* ATP-site competition binding assay (Karaman et al., 2008). **1a** was therefore picked to be further validated for STK19-targeted inhibition and experimental therapy in melanoma.

ZT-12-037-01 (**1a**) treatment efficiently inhibited phosphorylation of NRAS in a dose- and time-dependent manner (**Figures 5C and 5D**). Furthermore, with increasing ATP concentrations, the IC_{50} of **1a** against STK19 accordingly increased (**Figure 5E**), indicating that **1a** is an ATP-competitive inhibitor for STK19. **1a** also showed a high-affinity interaction with STK19 protein, as demonstrated by a shift of 6.8 °C in the melting temperature of STK19 (**Figure 5F**). To develop inhibitor-resistant alleles of STK19 that compromise the inhibitor binding, we performed a series of mutagenesis and biochemical studies based on the functional motifs and the hinge region (R131 to V150) within STK19. Introduction of single mutation of valine 134 to tyrosine (V134Y) or lysine 139 to phenylalanine (L139F) had minimal effects on STK19 kinase activity, but remarkably compromised the inhibitory potential of **1a** for STK19 (**Figures**

S5F and S5G). These results demonstrate that **1a** is on-target to STK19. We also found that **1a** has similar IC_{50} for $STK19^{WT}$ and $STK19^{D89N}$ (23.96 nM and 27.94 nM, respectively) (**Figure S5H**). The consistent inhibitory effects of **1a** on $STK19^{WT}$ and $STK19^{D89N}$-activated NRAS phosphorylation were also detected in HPMs (**Figure 5G**). These data suggest that the inhibitory ability of **1a** on STK19 was not dependent on a region around D89 within STK19. Importantly, **1a** did not affect mouse weight (**Figure S5I**), serum transaminase levels (**Table S2**) or histology of mouse tissues (**Figure S5J**), suggesting that ZT-12-037-01 (**1a**) is a highly potent STK19 inhibitor with low *in vivo* toxicity.

ZT-012-037-1 (1a) inhibits oncogenic NRAS-driven melanoma development and growth

To determine whether ZT-12-037-01 (**1a**) represented a potential therapeutic option for NRAS mutant melanoma, genetically engineered $NRAS^{Q61R}$-expressing human immortal melanocytes (hTERT/p53DD/CDK4(R24C)) ectopically expressing $STK19^{WT}$ or $STK19^{D89N}$ (**Figure S6A**) were treated with **1a**. We found that **1a** treatment significantly inhibited mutant NRAS/STK19-driven melanocyte colony formation (**Figure 6A**), proliferation (**Figure S6B**) and tumor formation (**Figures 6B-6D**). **1a** treatment also inhibited growth of SK-MEL-2 xenograft melanoma (with $NRAS^{Q61R}$) in a dose-dependent manner (**Figures 6E-6G**). We also performed immunofluorescence on SK-MEL-2 xenograft tumors to investigate the effects of **1a** on *in vivo* proliferation and apoptosis, represented by Ki67 and cleaved caspase-3 staining. We observed that **1a** treatment effectively inhibited cell proliferation and induced apoptosis of SK-MEL-2 tumors (**Figures 6H and 6I**), confirming the *in vivo* efficacy of **1a**. We then assessed the effects of **1a** on survival rate of SK-MEL-2 xenograft tumor-bearing mice and observed that **1a** significantly prolonged the survival of recipients compared with controls (**Figure S6C**). Taken together these data indicate the potential therapeutic benefits of targeting STK19 with ZT-12-037-01 (**1a**) in melanomas with mutant NRAS.

Next, we determined whether the treatment effects of **1a** are mediated by inhibiting NRAS signaling. Different doses of **1a** (0 μM, 1 μM, or 3 μM) were used to treat STK19-depleted HPMs ectopically expressing $NRAS^{Q61R}$ that were infected with retroviruses encoding empty Flag, Flag-tagged $STK19^{WT}$, or $STK19^{D89N}$. We found that **1a** effectively inhibited $STK19^{WT}$- and $STK19^{D89N}$-induced NRAS phosphorylation and activation of its downstream signaling (**Figure S6D**). We also collected SK-MEL-2 xenograft tumors with treatment of different doses of **1a** for immunoblot analysis to confirm that **1a** targeted STK19 to inhibit NRAS signaling but not G9a activity. Consistently, **1a** inhibited NRAS activity in a dose-dependent manner, but did not affect the levels of H3K9 methylation (**Figure S6E**), a downstream marker of G9a activity (Shinkai and Tachibana, 2011).

In addition, we investigated the growth inhibitory effects of **1a** in melanoma cells with different NRAS and BRAF status, including A375 and UACC62 ($NRAS^{WT}$, $BRAF^{V600E}$), and SK-MEL-2 and WM2032 ($NRAS^{Q61R}$, $BRAF^{WT}$). We found that **1a** effectively inhibited NRAS signaling, including the MEK-ERK and PI3K pathways in SK-MEL-2 and WM2032 cells (with $NRAS^{Q61R}$), but the inhibition was much less effective in A375 or UACC62 cells (with $NRAS^{WT}$) (**Figure S6F**). Consistently, **1a** effectively inhibited cell growth (**Figure S6G**) and induced apoptosis (**Figure S6H**) of SK-MEL-2 and WM2032 melanoma cells, but exhibited a reduced impact on A375 or UACC62 cells. These results indicate that pro-apoptotic effect of ZT-12-037-01 (**1a**) is dramatically enhanced in cells expressing oncogenic NRAS.

To confirm the specificity of the targeted inhibition of STK19 by **1a**, lower concentrations of **1a** (100 nM and 300 nM) were evaluated in SK-MEL-2 and WM2032 melanoma cells and the levels of H3K9 methylation and NRAS phosphorylation and activity were investigated by immunoblotting. We found up to 300 nM, **1a** had no obvious effects on H3K9 methylation but still effectively decreased NRAS phosphorylation and activity (**Figure S6I**). To further confirm the pharmacological effects of **1a** derive from STK19 inhibition and not G9a inhibition, we investigated the role of G9a in NRAS signaling

activation. G9a was silenced by G9a-specific shRNA or inhibited by a specific inhibitor, A-366, in SK-MEL-2 and WM2032 melanoma cells. We observed the inhibition of G9a activity by knockdown (**Figure S6J**) or treatment with A-366 (**Figure S6K**) markedly repressed H3K9 methylation levels but not NRAS signaling, indicating that **1a** inhibited NRAS activity via targeting STK19 but not G9a**.** We also found that **1a**-mediated inhibition of oncogenic NRAS signaling was rescued by introduction of **1a**-resistant STK19 V134Y or L139F, confirming the inhibition specificity of **1a** towards STK19 (**Figure S6L**). In summary, ZT-12-037-01 (**1a**) is a specific STK19-targeted inhibitor to block oncogenic NRAS-driven melanocyte malignant transformation and melanoma growth.

DISCUSSION

The development of targeted cancer therapies is facilitated by understanding the functional consequences of genetic driver mutations that lead to overactive signaling pathways. The three RAS genes (KRAS, HRAS and NRAS) are frequently activated by mutation in about 25% of all cancers including melanomas, pancreatic ductal adenocarcinomas, colorectal adenocarcinomas and lung adenocarcinomas (Cox et al., 2014; Lee et al., 2011; Stephen et al., 2014). Activating mutations in RAS family members and components of the downstream MEK/ERK signaling pathway also account for development of a group of genetic syndromes known as RASopathies (Rauen, 2013). However, unlike the downstream effectors of RAS, such as BRAF and MEK whose targeted therapy has been extensively exploited through the successful development of several small molecule inhibitors (Chapman et al., 2011; Flaherty et al., 2010; Kefford et al., 2010; Larkin et al., 2014; Long et al., 2017a, b), little progress has been made towards targeting activation of RAS proteins.

For example, since the activation of oncogenic RAS depends on the protein's localization at the inner face of plasma membrane for effector binding, efforts have been made towards targeting the hydrophobic

modifications of the C-terminal HVR domain necessary for RAS plasma membrane association (Ahearn et al., 2011; Barcelo et al., 2013; Berndt et al., 2011; Buss and Sefton, 1986; Casey et al., 1989; Wright and Philips, 2006). Moreover, the observation that RAS proteins are prenylated for plasma membrane localization and activation initially led to the development of farnesyltransferase inhibitors (FTIs) aimed at preventing RAS localization to the plasma membrane (Brunner et al., 2003). However, these attempts were unsuccessful in clinical trials because RAS proteins are also modified by geranylgeranyl isoprenoid to retain their membrane association (Karnoub and Weinberg, 2008). It has also recently been reported that a small molecule RAS-mimetic rigosertib and pan-RAS ligands block RAS binding to effector proteins, bringing new possibilities for anti-RAS therapy (Athuluri-Divakar et al., 2016; Welsch et al., 2017). In addition to these strategies, others have also considered targeting kinases/phosphatases that regulate RAS activity. Phosphorylation of NRAS at Y32 by the kinase SRC, which was recognized as a proto-oncogene protein to activate RAS and MEK/ERK signaling, was reported to inhibit RAS activity through GTP hydrolysis and dissociation of RAF binding (Bunda et al., 2014). Consequently, inhibition of SHP2 which mediates RAS dephosphorylation can suppress tumor growth in multiple cancers (Bunda et al., 2015; Mainardi et al., 2018; Wong et al., 2018). However, it remains to be seen whether these recent observations will be successfully translated to the clinic as therapies for cancers bearing oncogenic RAS.

In this study, rather than targeting RAS directly we identified and characterized the poorly studied serine/threonine kinase STK19 as a novel activator of NRAS. Our observations suggest that for activated NRAS to signal effectively and exert its oncogenic effects on melanocytes it needs to be phosphorylated on the S89 by STK19. Phosphorylation at S89 then promotes NRAS interaction with its downstream effector and accordingly STK19 activates NRAS signaling via the MEK/ERK and PI3K pathways. The identification of STK19 as a critical kinase upstream from NRAS prompted us to hypothesize that STK19 would represent a therapeutic vulnerability in NRAS-driven melanomas. Consistent with this, the selective STK19 inhibitor

ZT-12-037-01 (**1a**) developed here exhibits impressive inhibitory effects on STK19-induced NRAS phosphorylation and NRAS-driven melanoma progression *in vitro* and *in vivo*. Our results therefore offer a preclinical proof of concept for therapeutic targeting of the STK19 kinase in melanomas with NRAS mutations. Significantly, although we have focused on NRAS, we note that S89, the key residue in NRAS phosphorylated by STK19, is conserved in all the three RAS proteins. Since depletion or inhibition of STK19 limits the transforming potential of oncogenic NRAS in melanocytes and inhibits growth of NRAS mutant melanoma, our results suggest that targeting STK19 may represent a promising therapeutic approach for anti-RAS therapies in general.

Many different genetic driver mutations have been identified in melanomagenesis, most notably those affecting BRAF, NRAS, INK4a, PTEN and p14ARF (Fargnoli et al., 2008; Kim et al., 2008; Landi et al., 2006; Scherer et al.; Tsao et al., 2012). Our knowledge of driver genes in melanoma has recently been augmented by large-scale massively parallel sequencing studies that have identified additional significantly mutated genes include NF1, ARID2, PPP6C, SNX31, TACC1, STK19, and RAC1 from the initial large-scale melanoma exome data (Hodis et al., 2012; Krauthammer et al., 2012), as well as MAP2K1, IDH1, RB1, and DDX3X in the Cancer Genome Atlas Skin Cutaneous Melanoma (SKCM-TCGA) exome sequencing dataset (Akbani et al., 2015). Here our cellular and genetic studies extended these observations to identify the $STK19^{D89N}$ mutant as a gain-of-function mutation in melanomas which accelerates oncogenic NRAS-driven melanomagenesis *in vivo*. We also found that overexpression and mutations of STK19 were detected in about 25% of human melanomas and that higher STK19 expression conferred a substantially increased risk of mortality in patients with primary melanomas. However, no melanoma was observed in mice with an $STK19^{D89N}$ knockin alone. Our data therefore suggest that the STK19 mutant is not a typical driver, but is perhaps a helper mutation that facilitates melanoma development by activation of NRAS signaling. Notably, unlike those mutations activating NRAS

(Q61R/L/K) or BRAF (V600E), the significant hotspot D89N in STK19 corresponds to cytosine to a thymidine (C>T transition) UVR signature mutation in melanoma (Brash, 2015). As such our results may go some way to explain the association of NRAS mutation-associated melanoma with UVR if STK19 accelerates UVR-driven melanomagenesis in individuals with NRAS mutations.

Targeted therapies have significantly improved clinical outcomes in patients with various cancers such as BRAF inhibitors for metastatic melanoma and epidermal growth factor receptor (EGFR) inhibitors for EGFR mutant non-small cell lung cancer (NSCLC) (Chapman et al., 2011; Siegelin and Borczuk, 2014). However, the efficacy is almost always ultimately compromised by the acquisition of drug resistance, which frequently involves RAS mutations or reactivation of the MEK/ERK and PI3K pathways (Ercan et al., 2012; Hatzivassiliou et al., 2010). The ability to target RAS signaling using the STK19 inhibitor ZT-12-037-01 (**1a**) developed here might be further evaluated for rational integration of combination therapy to overcome or prevent drug-resistance in patients with RAS mutation cancers in future preclinical and ultimately clinical studies.

ACKNOWLEDGMENTS

We thank Drs. Norman Sharpless and David Fisher for kindly providing the loxP/STOP/loxP NRAS^{Q61R} knockin (LSL-NRAS^{Q61R}) mice. We thank Dr. Anurag Singh for kindly sharing cell lines. We also thank Drs. X. Shirley Liu, Tao Wang, Wantao Chen, Dali Liu, Chunxiao Xu, Jianming Zhang and Junrong Zou for discussion and assistance. This work was supported by grants from Boston University (to R.C.), the National Key R&D Program and the National Natural Science Foundation of China (No. 2017YFA0504504, 2016YFA0502001, 81422045, U1405223 and 81661138005 to X.D.), the Fundamental Research Funds for the Central Universities of China (No. 20720160064 to X.D.), and the Program of Introducing Talents of Discipline to Universities (111 Project, B12001).

AUTHOR CONTRIBUTIONS

Conceptualization, P.W., X.D., and R.C.; Methodology, C.Y., B.Z., T.Z., T.L., S.C., C.R.G., P.W., X.D., and R.C.; Formal Analysis, C.Y., B.Z., T.Z., T.L., S.C., X.L., J.Z., Z.W., P.W., X.D., and R.C.; Investigation, C.Y., B.Z., T.Z., T.L., S.C., X.L., X.M., S.L., X.M., J.Z., and L.L.; Writing-Original Draft, C.Y., B.Z., T.L., Y.,L, G.W., Z.X., X.G., C.H., C.R.G., P.W., X.D., and R.C.; Writing-Review & Editing, C.Y., B.Z., Z.W., C.R.G., P.W., X.D., and R.C.; Funding Acquisition, P.W., X.D., and R.C.; Resources, P.W., X.D., and R.C.; Supervision, P.W., X.D., and R.C.

DECLARATION OF INTERESTS

The authors declare no competing interests.

REFERENCES

Ackermann, J., Frutschi, M., Kaloulis, K., McKee, T., Trumpp, A., and Beermann, F. (2005). Metastasizing melanoma formation caused by expression of activated N-RasQ61K on an INK4a-deficient background. Cancer Res *65*, 4005-4011.

Ahearn, I.M., Haigis, K., Bar-Sagi, D., and Philips, M.R. (2011). Regulating the regulator: post-translational modification of RAS. Nat Rev Mol Cell Biol *13*, 39-51.

Akbani, R., Akdemir, K.C., Aksoy, B.A., Albert, M., Ally, A., Amin, S.B., Arachchi, H., Arora, A., Auman, J.T., Ayala, B.*, et al.* (2015). Genomic Classification of Cutaneous Melanoma. Cell *161*, 1681-1696.

Athuluri-Divakar, S.K., Vasquez-Del Carpio, R., Dutta, K., Baker, S.J., Cosenza, S.C., Basu, I., Gupta, Y.K., Reddy, M.V., Ueno, L., Hart, J.R.*, et al.* (2016). A Small Molecule RAS-Mimetic Disrupts RAS Association with Effector Proteins to Block Signaling. Cell *165*, 643-655.

Bacher, U., Haferlach, T., Schoch, C., Kern, W., and Schnittger, S. (2006). Implications of NRAS mutations in AML: a study of 2502 patients. Blood *107*, 3847-3853.

Barbacid, M. (1987). ras genes. Annu Rev Biochem *56*, 779-827.

Barcelo, C., Paco, N., Beckett, A.J., Alvarez-Moya, B., Garrido, E., Gelabert, M., Tebar, F., Jaumot, M., Prior, I., and Agell, N. (2013). Oncogenic K-ras segregates at spatially distinct plasma membrane signaling platforms according to its phosphorylation status. J Cell Sci *126*, 4553-4559.

Barcelo, C., Paco, N., Morell, M., Alvarez-Moya, B., Bota-Rabassedas, N., Jaumot, M., Vilardell, F., Capella, G., and Agell, N. (2014). Phosphorylation at Ser-181 of Oncogenic KRAS Is Required for Tumor Growth. Cancer Research *74*, 1190-1199.

Barretina, J., Caponigro, G., Stransky, N., Venkatesan, K., Margolin, A.A., Kim, S., Wilson, C.J., Lehar, J., Kryukov, G.V., Sonkin, D.*, et al.* (2012). The Cancer Cell Line Encyclopedia enables predictive modelling of anticancer drug sensitivity. Nature *483*, 603-607.

Berger, M.F., Hodis, E., Heffernan, T.P., Deribe, Y.L., Lawrence, M.S., Protopopov, A., Ivanova, E., Watson, I.R., Nickerson, E., Ghosh, P.*, et al.* (2012). Melanoma genome sequencing reveals frequent PREX2 mutations. Nature *485*, 502-506.
Berndt, N., Hamilton, A.D., and Sebti, S.M. (2011). Targeting protein prenylation for cancer therapy. Nature Reviews Cancer *11*, 775-791.
Boeing, S., Williamson, L., Encheva, V., Gori, I., Saunders, R.E., Instrell, R., Aygun, O., Rodriguez-Martinez, M., Weems, J.C., Kelly, G.P.*, et al.* (2016). Multiomic Analysis of the UV-Induced DNA Damage Response. Cell Rep *15*, 1597-1610.
Bonilla, X., Parmentier, L., King, B., Bezrukov, F., Kaya, G., Zoete, V., Seplyarskiy, V.B., Sharpe, H.J., McKee, T., Letourneau, A.*, et al.* (2016). Genomic analysis identifies new drivers and progression pathways in skin basal cell carcinoma. Nat Genet *48*, 398-406.
Bos, J.L. (1989). ras oncogenes in human cancer: a review. Cancer Res *49*, 4682-4689.
Brash, D.E. (2015). UV signature mutations. Photochem Photobiol *91*, 15-26.
Brunner, T.B., Hahn, S.M., Gupta, A.K., Muschel, R.J., McKenna, W.G., and Bernhard, E.J. (2003). Farnesyltransferase inhibitors: an overview of the results of preclinical and clinical investigations. Cancer Res *63*, 5656-5668.
Bunda, S., Burrell, K., Heir, P., Zeng, L., Alamsahebpour, A., Kano, Y., Raught, B., Zhang, Z.Y., Zadeh, G., and Ohh, M. (2015). Inhibition of SHP2-mediated dephosphorylation of Ras suppresses oncogenesis. Nat Commun *6*, 8859.
Bunda, S., Heir, P., Srikumar, T., Cook, J.D., Burrell, K., Kano, Y., Lee, J.E., Zadeh, G., Raught, B., and Ohh, M. (2014). Src promotes GTPase activity of Ras via tyrosine 32 phosphorylation. P Natl Acad Sci USA *111*, E3785-E3794.
Burd, C.E., Liu, W., Huynh, M.V., Waqas, M.A., Gillahan, J.E., Clark, K.S., Fu, K., Martin, B.L., Jeck, W.R., Souroullas, G.P.*, et al.* (2014a). Mutation-Specific RAS Oncogenicity Explains NRAS Codon 61 Selection in Melanoma. Cancer Discov *4*, 1418-1429.
Burd, C.E., Liu, W., Huynh, M.V., Waqas, M.A., Gillahan, J.E., Clark, K.S., Fu, K., Martin, B.L., Jeck, W.R., Souroullas, G.P.*, et al.* (2014b). Mutation-specific RAS oncogenicity explains NRAS codon 61 selection in melanoma. Cancer Discov *4*, 1418-1429.
Buss, J.E., and Sefton, B.M. (1986). Direct Identification of Palmitic Acid as the Lipid Attached to P21ras. Mol Cell Biol *6*, 116-122.
Casey, P.J., Solski, P.A., Der, C.J., and Buss, J.E. (1989). P21ras Is Modified by a Farnesyl Isoprenoid. P Natl Acad Sci USA *86*, 8323-8327.
Chapman, P.B., Hauschild, A., Robert, C., Haanen, J.B., Ascierto, P., Larkin, J., Dummer, R., Garbe, C., Testori, A., Maio, M.*, et al.* (2011). Improved survival with vemurafenib in melanoma with BRAF V600E mutation. N Engl J Med *364*, 2507-2516.
Chen, S., Zhu, B., Yin, C., Liu, W., Han, C., Chen, B., Liu, T., Li, X., Chen, X., Li, C.*, et al.* (2017). Palmitoylation-dependent activation of MC1R prevents melanomagenesis. Nature *549*, 399-403.
Chiu, V.K., Bivona, T., Hach, A., Sajous, J.B., Silletti, J., Wiener, H., Johnson, R.L., Cox, A.D., and Philips, M.R. (2002). Ras signalling on the endoplasmic reticulum and the Golgi. Nat Cell Biol *4*, 343-350.
Chu, V., Weber, T., Graf, R., Sommermann, T., Petsch, K., Sack, U., Volchkov, P., Rajewsky, K., and Kuhn, R. (2016). Efficient generation of Rosa26 knock-in mice using CRISPR/Cas9 in C57BL/6 zygotes. Bmc Biotechnol *16*.
Cox, A.D., Fesik, S.W., Kimmelman, A.C., Luo, J., and Der, C.J. (2014). Drugging the undruggable RAS: Mission possible? Nat Rev Drug Discov *13*, 828-851.
Dankort, D., Curley, D.P., Cartlidge, R.A., Nelson, B., Karnezis, A.N., Damsky, W.E., You, M.J., DePinho, R.A., McMahon, M., and Bosenberg, M. (2009). Braf(V600E) cooperates with Pten loss to induce metastatic melanoma. Nature Genetics *41*, 544-552.
Davies, H., Bignell, G.R., Cox, C., Stephens, P., Edkins, S., Clegg, S., Teague, J., Woffendin, H., Garnett, M.J., Bottomley, W.*, et al.* (2002). Mutations of the BRAF gene in human cancer. Nature *417*, 949-954.
Downward, J. (2003). Targeting RAS signalling pathways in cancer therapy. Nat Rev Cancer *3*, 11-22.

Ercan, D., Xu, C., Yanagita, M., Monast, C.S., Pratilas, C.A., Montero, J., Butaney, M., Shimamura, T., Sholl, L., Ivanova, E.V.*, et al.* (2012). Reactivation of ERK signaling causes resistance to EGFR kinase inhibitors. Cancer Discov *2*, 934-947.
Fargnoli, M.C., Pike, K., Pfeiffer, R.M., Tsang, S., Rozenblum, E., Munroe, D.J., Golubeva, Y., Calista, D., Seidenari, S., Massi, D.*, et al.* (2008). MC1R variants increase risk of melanomas harboring BRAF mutations. J Invest Dermatol *128*, 2485-2490.
Flaherty, K.T., Puzanov, I., Kim, K.B., Ribas, A., McArthur, G.A., Sosman, J.A., O'Dwyer, P.J., Lee, R.J., Grippo, J.F., Nolop, K.*, et al.* (2010). Inhibition of Mutated, Activated BRAF in Metastatic Melanoma. New Engl J Med *363*, 809-819.
Garraway, L.A., Widlund, H.R., Rubin, M.A., Getz, G., Berger, A.J., Ramaswamy, S., Beroukhim, R., Milner, D.A., Granter, S.R., Du, J.Y.*, et al.* (2005). Integrative genomic analyses identify MITF as a lineage survival oncogene amplified in malignant melanoma. Nature *436*, 117-122.
Goel, V.K., Lazar, A.J., Warneke, C.L., Redston, M.S., and Haluska, F.G. (2006). Examination of mutations in BRAF, NRAS, and PTEN in primary cutaneous melanoma. J Invest Dermatol *126*, 154-160.
Gomez-Escobar, N., Chou, C.F., Lin, W.W., Hsieh, S.L., and Campbell, R.D. (1998). The G11 gene located in the major histocompatibility complex encodes a novel nuclear serine/threonine protein kinase. J Biol Chem *273*, 30954-30960.
Hatzivassiliou, G., Song, K., Yen, I., Brandhuber, B.J., Anderson, D.J., Alvarado, R., Ludlam, M.J., Stokoe, D., Gloor, S.L., Vigers, G.*, et al.* (2010). RAF inhibitors prime wild-type RAF to activate the MAPK pathway and enhance growth. Nature *464*, 431-435.
Hayward, N.K., Wilmott, J.S., Waddell, N., Johansson, P.A., Field, M.A., Nones, K., Patch, A.M., Kakavand, H., Alexandrov, L.B., Burke, H.*, et al.* (2017). Whole-genome landscapes of major melanoma subtypes. Nature *545*, 175-180.
Herlyn, M., Thurin, J., Balaban, G., Bennicelli, J.L., Herlyn, D., Elder, D.E., Bondi, E., Guerry, D., Nowell, P., Clark, W.H.*, et al.* (1985). Characteristics of cultured human melanocytes isolated from different stages of tumor progression. Cancer Res *45*, 5670-5676.
Hodis, E., Watson, I.R., Kryukov, G.V., Arold, S.T., Imielinski, M., Theurillat, J.P., Nickerson, E., Auclair, D., Li, L., Place, C.*, et al.* (2012). A landscape of driver mutations in melanoma. Cell *150*, 251-263.
Hugo, W., Zaretsky, J.M., Sun, L., Song, C., Moreno, B.H., Hu-Lieskovan, S., Berent-Maoz, B., Pang, J., Chmielowski, B., Cherry, G.*, et al.* (2016). Genomic and Transcriptomic Features of Response to Anti-PD-1 Therapy in Metastatic Melanoma. Cell *165*, 35-44.
Jackson, J.H., Cochrane, C.G., Bourne, J.R., Solski, P.A., Buss, J.E., and Der, C.J. (1990). Farnesol Modification of Kirsten-Ras Exon 4b-Protein Is Essential for Transformation. P Natl Acad Sci USA *87*, 3042-3046.
Jakob, J.A., Bassett, R.L., Ng, C.S., Curry, J.L., Joseph, R.W., Alvarado, G.C., Rohlfs, M.L., Richard, J., Gershenwald, J.E., Kim, K.B.*, et al.* (2012). NRAS mutation status is an independent prognostic factor in metastatic melanoma. Cancer-Am Cancer Soc *118*, 4014-4023.
Ji, Z., Flaherty, K.T., and Tsao, H. (2012). Targeting the RAS pathway in melanoma. Trends Mol Med *18*, 27-35.
Karaman, M.W., Herrgard, S., Treiber, D.K., Gallant, P., Atteridge, C.E., Campbell, B.T., Chan, K.W., Ciceri, P., Davis, M.I., Edeen, P.T.*, et al.* (2008). A quantitative analysis of kinase inhibitor selectivity. Nat Biotechnol *26*, 127-132.
Karnoub, A.E., and Weinberg, R.A. (2008). Ras oncogenes: split personalities. Nat Rev Mol Cell Biol *9*, 517-531.
Kawakami, Y., Kitaura, J., Yao, L., McHenry, R.W., Kawakami, Y., Newton, A.C., Kang, S., Kato, R.M., Leitges, M., Rawlings, D.J.*, et al.* (2003). A Ras activation pathway dependent on Syk phosphorylation of protein kinase C. Proc Natl Acad Sci U S A *100*, 9470-9475.
Kefford, R., Arkenau, H., Brown, M.P., Millward, M., Infante, J.R., Long, G.V., Ouellet, D., Curtis, M., Lebowitz, P.F., and Falchook, G.S. (2010). Phase I/II study of GSK2118436, a selective inhibitor of oncogenic mutant BRAF kinase, in patients with metastatic melanoma and other solid tumors. J Clin Oncol *28*.
Kim, R.D., Curtin, J.A., and Bastian, B.C. (2008). Lack of somatic alterations of MC1R in primary melanoma. Pigment Cell Melanoma Res *21*, 579-582.

Krauthammer, M., Kong, Y., Ha, B.H., Evans, P., Bacchiocchi, A., McCusker, J.P., Cheng, E., Davis, M.J., Goh, G., Choi, M.*, et al.* (2012). Exome sequencing identifies recurrent somatic RAC1 mutations in melanoma. Nat Genet *44*, 1006-1014.
Krengel, U., Schlichting, I., Scherer, A., Schumann, R., Frech, M., John, J., Kabsch, W., Pai, E.F., and Wittinghofer, A. (1990). 3-Dimensional Structures of H-Ras P21 Mutants - Molecular-Basis for Their Inability to Function as Signal Switch Molecules. Cell *62*, 539-548.
Landi, M.T., Bauer, J., Pfeiffer, R.M., Elder, D.E., Hulley, B., Minghetti, P., Calista, D., Kanetsky, P.A., Pinkel, D., and Bastian, B.C. (2006). MC1R germline variants confer risk for BRAF-mutant melanoma. Science *313*, 521-522.
Larkin, J., Ascierto, P.A., Dreno, B., Atkinson, V., Liszkay, G., Maio, M., Mandala, M., Demidov, L., Stroyakovskiy, D., Thomas, L.*, et al.* (2014). Combined vemurafenib and cobimetinib in BRAF-mutated melanoma. N Engl J Med *371*, 1867-1876.
Lavoie, H., and Therrien, M. (2015). Regulation of RAF protein kinases in ERK signalling. Nat Rev Mol Cell Biol *16*, 281-298.
Lawrence, M.S., Stojanov, P., Mermel, C.H., Robinson, J.T., Garraway, L.A., Golub, T.R., Meyerson, M., Gabriel, S.B., Lander, E.S., and Getz, G. (2014). Discovery and saturation analysis of cancer genes across 21 tumour types. Nature *505*, 495-501.
Lee, J.H., Choi, J.W., and Kim, Y.S. (2011). Frequencies of BRAF and NRAS mutations are different in histological types and sites of origin of cutaneous melanoma: a meta-analysis. Br J Dermatol *164*, 776-784.
Lissanu Deribe, Y., Shi, Y., Rai, K., Nezi, L., Amin, S.B., Wu, C.C., Akdemir, K.C., Mahdavi, M., Peng, Q., Chang, Q.E.*, et al.* (2016). Truncating PREX2 mutations activate its GEF activity and alter gene expression regulation in NRAS-mutant melanoma. Proc Natl Acad Sci U S A *113*, E1296-1305.
Liu, F., Barsyte-Lovejoy, D., Li, F.L., Xiong, Y., Korboukh, V., Huang, X.P., Allali-Hassani, A., Janzen, W.P., Roth, B.L., Frye, S.V.*, et al.* (2013). Discovery of an in Vivo Chemical Probe of the Lysine Methyltransferases G9a and GLP. J Med Chem *56*, 8931-8942.
Long, G.V., Hauschild, A., Santinami, M., Atkinson, V., Mandala, M., Chiarion-Sileni, V., Larkin, J., Nyakas, M., Dutriaux, C., Haydon, A.*, et al.* (2017a). Adjuvant Dabrafenib plus Trametinib in Stage III BRAF-Mutated Melanoma. N Engl J Med.
Long, G.V., Hauschild, A., Santinami, M., Atkinson, V., Mandala, M., Chiarion-Sileni, V., Larkin, J., Nyakas, M., Dutriaux, C., Haydon, A.*, et al.* (2017b). Adjuvant Dabrafenib plus Trametinib in Stage III BRAF-Mutated Melanoma. N Engl J Med *377*, 1813-1823.
Mainardi, S., Mulero-Sanchez, A., Prahallad, A., Germano, G., Bosma, A., Krimpenfort, P., Lieftink, C., Steinberg, J.D., de Wit, N., Goncalves-Ribeiro, S.*, et al.* (2018). SHP2 is required for growth of KRAS-mutant non-small-cell lung cancer in vivo. Nat Med.
Malumbres, M., and Barbacid, M. (2003). RAS oncogenes: the first 30 years. Nat Rev Cancer *3*, 459-465.
Marais, R., Light, Y., Paterson, H.F., and Marshall, C.J. (1995). Ras recruits Raf-1 to the plasma membrane for activation by tyrosine phosphorylation. EMBO J *14*, 3136-3145.
Mendoza, M.C., Er, E.E., and Blenis, J. (2011). The Ras-ERK and PI3K-mTOR pathways: cross-talk and compensation. Trends Biochem Sci *36*, 320-328.
Milburn, M.V., Tong, L., Devos, A.M., Brunger, A., Yamaizumi, Z., Nishimura, S., and Kim, S.H. (1990). Molecular Switch for Signal Transduction - Structural Differences between Active and Inactive Forms of Protooncogenic Ras Proteins. Science *247*, 939-945.
Prior, I.A., Lewis, P.D., and Mattos, C. (2012). A comprehensive survey of Ras mutations in cancer. Cancer Res *72*, 2457-2467.
Pylayeva-Gupta, Y., Grabocka, E., and Bar-Sagi, D. (2011). RAS oncogenes: weaving a tumorigenic web. Nat Rev Cancer *11*, 761-774.
Rauen, K.A. (2013). The RASopathies. Annu Rev Genomics Hum Genet *14*, 355-369.
Samatar, A.A., and Poulikakos, P.I. (2014). Targeting RAS-ERK signalling in cancer: promises and challenges. Nat Rev Drug Discov *13*, 928-942.

Sargent, C.A., Anderson, M.J., Hsieh, S.L., Kendall, E., Gomez-Escobar, N., and Campbell, R.D. (1994). Characterisation of the novel gene G11 lying adjacent to the complement C4A gene in the human major histocompatibility complex. Hum Mol Genet *3*, 481-488.
Scherer, D., Rachakonda, P.S., Angelini, S., Mehnert, F., Sucker, A., Egberts, F., Hauschild, A., Hemminki, K., Schadendorf, D., and Kumar, R. Association between the germline MC1R variants and somatic BRAF/NRAS mutations in melanoma tumors. J Invest Dermatol *130*, 2844-2848.
Shinkai, Y., and Tachibana, M. (2011). H3K9 methyltransferase G9a and the related molecule GLP. Genes Dev *25*, 781-788.
Siegelin, M.D., and Borczuk, A.C. (2014). Epidermal growth factor receptor mutations in lung adenocarcinoma. Lab Invest *94*, 129-137.
Smith, M.J., Neel, B.G., and Ikura, M. (2013). NMR-based functional profiling of RASopathies and oncogenic RAS mutations. Proc Natl Acad Sci U S A *110*, 4574-4579.
Stephen, A.G., Esposito, D., Bagni, R.K., and McCormick, F. (2014). Dragging ras back in the ring. Cancer Cell *25*, 272-281.
Sweis, R.F., Pliushchev, M., Brown, P.J., Guo, J., Li, F., Maag, D., Petros, A.M., Soni, N.B., Tse, C., Vedadi, M.*, et al.* (2014). Discovery and development of potent and selective inhibitors of histone methyltransferase g9a. ACS Med Chem Lett *5*, 205-209.
Ting, P.Y., Johnson, C.W., Fang, C., Cao, X.Q., Graeber, T.G., Mattos, C., and Colicelli, J. (2015). Tyrosine phosphorylation of RAS by ABL allosterically enhances effector binding. Faseb J *29*, 3750-3761.
Tsao, H., Chin, L., Garraway, L.A., and Fisher, D.E. (2012). Melanoma: from mutations to medicine. Genes Dev *26*, 1131-1155.
Wan, P.T., Garnett, M.J., Roe, S.M., Lee, S., Niculescu-Duvaz, D., Good, V.M., Jones, C.M., Marshall, C.J., Springer, C.J., Barford, D.*, et al.* (2004). Mechanism of activation of the RAF-ERK signaling pathway by oncogenic mutations of B-RAF. Cell *116*, 855-867.
Wellbrock, C., Ogilvie, L., Hedley, D., Karasarides, M., Martin, J., Niculescu-Duvaz, D., Springer, C.J., and Marais, R. (2004). B-V599E-RAF is an oncogene in melanocytes. Cancer Research *64*, 2338-2342.
Welsch, M.E., Kaplan, A., Chambers, J.M., Stokes, M.E., Bos, P.H., Zask, A., Zhang, Y., Sanchez-Martin, M., Badgley, M.A., Huang, C.S.*, et al.* (2017). Multivalent Small-Molecule Pan-RAS Inhibitors. Cell *168*, 878-889 e829.
Wong, G.S., Zhou, J., Liu, J.B., Wu, Z., Xu, X., Li, T., Xu, D., Schumacher, S.E., Puschhof, J., McFarland, J.*, et al.* (2018). Targeting wild-type KRAS-amplified gastroesophageal cancer through combined MEK and SHP2 inhibition. Nat Med.
Wright, L.P., and Philips, M.R. (2006). Thematic review series: lipid posttranslational modifications. CAAX modification and membrane targeting of Ras. J Lipid Res *47*, 883-891.

FIGURE LEGENDS

Figure 1. STK19 is a critical regulator of NRAS function.

A. Strategy used for identification of kinases regulating $NRAS^{Q61R}$-effector protein:protein interaction.

B. Whole-kinome screen identifies STK19 as a novel regulator of $NRAS^{Q61R}$ activity. Active NRAS chemiluminescence assay was performed to screen a total of 709 kinases whose knockdown affects interaction between $NRAS^{Q61R}$ and GST-CRAF RBD fusion protein. Vertical axis represents relative level

of active NRAS compared to group treated with control siRNA. Data are means of three individual kinase-targeting siRNA.

C. STK19 alterations were identified in 25.07% of 363 melanoma cases (TCGA, PanCancer Atlas).

D. STK19 was depleted in human primary melanocytes infected with retroviruses encoding empty HA, HA-NRAS^{WT}, or HA-NRAS^{Q61R}. Active HA-NRAS proteins were pulled down by GST-CRAF RBD fusion protein. Active HA-NRAS levels and activation of NRAS downstream signaling were detected by immunoblots. shCTRL, non-targeting shRNA. shSTK19, shRNA targeting STK19.

E. hTERT/p53DD/CDK4(R24C) melanocytes expressing empty HA, HA-NRAS^{WT} or HA-NRAS^{Q61R} were introduced with control shRNA or STK19 shRNA, and then seeded for colony formation assay. Data are means ± SD relative to control group with control shRNA and empty HA (n=6).

F-H. Growth curve, tumor weight, and dissected tumors for the xenograft experiments with indicated cells inoculated subcutaneously into flanks of nude mice. Visible tumors were measured every three days. Data are means ± SEM relative to control group (n=6).

See also Figure S1.

Figure 2. STK19 phosphorylates NRAS protein at serine 89.

A. Mass spectral peptide count of STK19-interacting proteins.

B-C. Exogenous interactions between HA-NRAS and STK19-Flag were detected by immunoprecipitation in HPMs with overexpression of STK19-Flag and empty HA, HA-NRAS^{WT} or HA-NRAS^{Q61R}.

D. HPMs were introduced with retroviruses encoding empty HA, HA-NRAS^{WT} or HA-NRAS^{Q61R} and/or STK19-Flag. The serine-, threonine- and tyrosine-phosphorylation of HA-NRAS isoforms were detected by immunoblots with specific antibodies.

E. Mass spectrometry analysis to identify serine 89 (S89) as the phosphorylation residue by STK19.

F. Schematic diagram showing the evolutionarily conserved serine residue (S89) in NRAS.

G. An *in vitro* kinase assay was performed using purified recombinant human STK19 protein and indicated purified recombinant human NRAS isoform proteins, followed by detection of phosphorylation in NRAS.

H. HPMs were introduced with empty HA, HA-NRAS^{WT}, HA-NRAS^{S89A}, HA-NRAS^{Q61R}, or HA-NRAS$^{Q61R/S89A}$. The NRAS-effector protein:protein interaction (including BRAF, CRAF and PI3Kα), active HA-NRAS levels and activation of NRAS downstream signaling were detected by immunoblots after infection with retroviruses encoding empty Flag or Flag-tagged STK19.

I. hTERT/p53DD/CDK4(R24C) melanocytes expressing empty HA, HA-NRAS^{Q61R} or HA-NRAS$^{Q61R/S89A}$ were introduced with retroviruses encoding empty Flag or Flag-tagged STK19, and then seeded for colony formation assay. Data are means ± SD relative to control group with empty HA vector and empty Flag vector (n=6).

J-L. Growth curve, tumor weight, and dissected tumors for the xenograft experiments with indicated cells inoculated subcutaneously into flanks of nude mice. Visible tumors were measured every three days. Data are means ± SEM relative to control group (n=7).

See also Figures S2.

Figure 3. STK19 D89N is a recurrent gain-of-function mutation.

A. STK19 mutations in TCGA database.

B. An *in vitro* kinase assay was performed using purified recombinant human STK19^{WT} and STK19^{D89N} proteins and indicated human NRAS isoform proteins, followed by detection of phosphorylation in NRAS.

C. HPMs with depletion of STK19 and overexpression of empty HA, HA-NRAS^{WT}, or HA-NRAS^{Q61R} were further infected with retroviruses encoding empty Flag, Flag-tagged STK19^{WT} or STK19^{D89N}. Serine

phosphorylation of HA-NRAS, active HA-NRAS levels and activation of NRAS downstream signaling were detected by immunoblots.

D. hTERT/p53DD/CDK4(R24C) melanocytes expressing STK19 shRNA and empty HA, HA-NRAS^{WT} or HA-NRAS^{Q61R} were introduced with retroviruses encoding empty Flag, Flag-tagged STK19^{WT} or STK19^{D89N}, and then seeded for colony formation assay. Data are means ± SD relative to control group with empty HA vector and empty Flag vector (n=6).

E-G. Growth curve, tumor weight, and dissected tumors for the xenograft experiments with indicated cells inoculated subcutaneously into flanks of nude mice. Visible tumors were measured every three days. Data are means ± SEM relative to control group (n=6).

See also Figure S3.

Figure 4. STK19 D89N induces melanomagenesis in the presence of oncogenic NRAS *in vivo.*

A. Tyr-Cre, Tyr-Cre-STK19^{WT} and Tyr-Cre-STK19^{D89N} knockin mice.

B. Ears of Tyr-Cre, Tyr-Cre-STK19^{WT} and Tyr-Cre-STK19^{D89N} knockin mice.

C. Tails of Tyr-Cre, Tyr-Cre-STK19^{WT} and Tyr-Cre-STK19^{D89N} knockin mice.

D. Fontana Masson staining of indicated mouse ears.

E. Quantification of skin melanin content in Tyr-Cre, Tyr-Cre-STK19^{WT} and Tyr-Cre-STK19^{D89N} knockin mice. Data are means ± SD relative to Tyr-Cre control group (n=3).

F. Primary mouse melanocytes derived from indicated mice were lysed for immunoblot analysis of human STK19 expression and NRAS signaling pathways after treatment of 4-hydroxytamoxifen (4-OHT).

G. Melanoma-free survival. Tyr-Cre, n=20; Tyr-Cre-NRAS^{Q61R}, n=18; Tyr-Cre-STK19^{WT}, n=19; Tyr-Cre-STK19^{D89N}, n=20; Tyr-Cre-NRAS^{Q61R}-STK19^{WT}, n=19; Tyr-Cre-NRAS^{Q61R}-STK19^{D89N}, n=19. By log-rank test, P=0.0116 (Tyr-Cre-NRAS^{Q61R}, Tyr-Cre-NRAS^{Q61R}-STK19^{WT}), P<0.001 (Tyr-Cre-

$NRAS^{Q61R}$, Tyr-Cre-$NRAS^{Q61R}$-$STK19^{D89N}$), *P*=0.0269 (Tyr-Cre-$NRAS^{Q61R}$-$STK19^{WT}$, Tyr-Cre-NRAS Q61R-$STK19^{D89N}$).

See also Figure S4.

Figure 5. Development of ZT-012-037-1 (1a) as a specific small molecule STK19 inhibitor.

A. The chemical structure of ZT-012-037-1 (**1a**).

B. The inhibitory activity of MP-IN-317 and **1a** for STK19, measured as percentage of NRAS phosphorylation. Data are means ± SD relative to control group (n = 3). IC_{50} represents median inhibitory concentration.

C-D. Phosphorylation of HA-$NRAS^{Q61R}$ was detected by immunoblots with an *in vitro* kinase assay at different doses of **1a** for 15 min or 3 μM of ZT-012-037-1 for different reaction time.

E. IC_{50} values of **1a** against STK19 at different ATP concentrations. Data are means ± SD relative to control groups (n = 3).

F. The thermal denaturation curve shift of STK19 (10 μM) in the presence of **1a** (100 μM).

G. Immunoblots to detect inhibition of $STK19^{WT}$ and $STK19^{D89N}$ by **1a** at different concentrations.

See also Figure S5, Tables S1 and S2.

Figure 6. ZT-012-037-1 (1a) inhibits oncogenic NRAS-driven melanoma development and growth.

A. hTERT/p53DD/CDK4(R24C) melanocytes induced with STK19 shRNA and retroviruses encoding empty Flag, Flag-tagged $STK19^{WT}$ or $STK19^{D89N}$ were treated with 3 μM **1a** or not, and proceeded for colony formation assay. Data are means ± SD relative to control group (n=6).

B-D. Growth curve, tumor weight, and dissected tumors for the xenograft experiments with indicated cells inoculated subcutaneously into flanks of nude mice treated with **1a**. Visible tumors were measured every three days. Data are means ± SEM relative to control group (n=6).

E-G. Growth curve, tumor weight, and dissected tumors for the xenograft experiments with SK-MEL-2 cells inoculated subcutaneously into flanks of nude mice treated with **1a**. Visible tumors were measured every three days. Data are means ± SEM relative to control group (n=7).

H-I. Effects of **1a** treatment on *in vivo* proliferation and apoptosis were evaluated by staining of the sections of tumor collected in **G** for Ki67 and cleaved caspase-3. The sections were counterstained with DAPI. Data are means ± SD (n=7). Representative images were shown. Scale bar, 100 μm.

See also Figures S6.

SUPPLEMENTAL FIGURE LEGENDS

Figure S1. STK19 is a critical regulator of NRAS function, related to Figure 1.

A. Mutual exclusivity between STK19 and BRAF alterations in TCGA PanCancer Atlas.

B. STK19 was depleted in A375, UACC62, SK-MEL-2 and WM2032 cells. Active NRAS proteins were pulled down by GST-CRAF RBD fusion protein. Active NRAS levels and activation of NRAS downstream signaling were detected by immunoblots.

C. STK19 was depleted in HPM, A375, UACC62, SK-MEL-2 and WM2032 cells, and the cell proliferation rates were measured. Data are means ± SD relative to individual control group (n=6).

D. qRT-PCR analysis of STK19 mRNA levels in SK-MEL-2 and WM2032 cells infected with STK19 shRNAs. Error bars indicate 95% confidence interval of triplicates.

E. STK19 was depleted in SK-MEL-2 and WM2032 cells. Active NRAS proteins were pulled down by GST-CRAF RBD fusion protein. Active NRAS levels and activation of NRAS downstream signaling were detected by immunoblots.

F. SK-MEL-2 and WM2032 cells with depletion of STK19 were infected with retroviruses encoding empty Flag or Flag-tagged STK19^{WT}. Active NRAS proteins were pulled down by GST-CRAF RBD fusion protein. Active NRAS levels and activation of NRAS downstream signaling were detected by immunoblots.

G. Immunoblots to show depletion of STK19 and overexpression of HA-NRAS proteins in hTERT/p53DD/CDK4(R24C) melanocytes.

H. hTERT/p53DD/CDK4(R24C) melanocytes expressing empty HA, HA-NRAS^{WT} or HA-NRAS^{Q61R} were introduced with control shRNA or STK19 shRNA, and then seeded for cell proliferation assay. Data are means ± SD relative to control group (n=6).

Figure S2. STK19 phosphorylates NRAS protein at serine 89, related to Figure 2.

A. Strategy to identify STK19-interacting proteins by mass spectrometry analysis.

B-C. Endogenous STK19-NRAS interactions were detected by immunoprecipitation in SK-MEL-2, WM2032, A375 and UACC62 cells.

D. The serine phosphorylation of NRAS in a panel of melanoma cells was detected by immunoblots.

E. STK19 was depleted by shSTK19 in HPMs overexpressing empty HA, HA-NRAS^{WT}, or HA-NRAS^{Q61R}. The serine phosphorylation of HA-NRAS was detected by immunoblots.

F. The serine phosphorylation of NRAS was detected by immunoblots in SK-MEL-2 and WM2032 cells with depletion of endogenous STK19.

G. HPMs with depletion of STK19 and overexpression of HA-tagged empty vector, HA-NRAS^{WT}, or HA-NRAS^{Q61R} were further infected with retroviruses encoding Flag tagged empty vector, Flag-tagged STK19^{WT} or kinase-dead STK19^{K317P}. The serine phosphorylation of HA-NRAS and STK19-NRAS interactions were detected by immunoblots.

H. The serine phosphorylation of NRAS was detected by immunoblots in SK-MEL-2 and WM2032 cells with depletion of endogenous STK19 and overexpression of empty Flag, Flag-tagged $STK19^{WT}$ or kinase dead $STK19^{K317P}$.

I. An *in vitro* kinase assay was performed using purified recombinant human STK19 protein and human NRAS (WT and Q61R) protein followed by detection of phosphorylation in NRAS.

J. Purified recombinant human NRAS protein preloaded with GDP, GTP or GTPγS were incubated with purified recombinant human STK19 protein for *in vitro* kinase assay followed by detection of phosphorylation in NRAS.

K. HPMs were transduced with indicated NRAS mutant isoforms and Flag-tagged STK19. The serine phosphorylation of HA-NRAS and STK19-NRAS interactions were detected by immunoblots.

L. HPMs were transduced with empty HA, HA-$NRAS^{WT}$, HA-$NRAS^{S89D}$, HA-$NRAS^{Q61R}$, or HA-$NRAS^{Q61R/S89D}$. The NRAS-effector protein:protein interaction (including BRAF, CRAF and PI3Kα), active HA-NRAS levels and activation of NRAS downstream signaling were detected by immunoblots.

M. Immunoblots to show overexpression of HA-NRAS and STK19-Flag isoforms in hTERT/p53DD/CDK4(R24C) melanocytes.

N. hTERT/p53DD/CDK4(R24C) melanocytes expressing empty HA, HA-$NRAS^{WT}$, HA-$NRAS^{S89A}$, HA-$NRAS^{Q61R}$ or HA-$NRAS^{Q61R/S89A}$ were introduced with retroviruses encoding empty Flag or Flag-tagged STK19, and then seeded for cell proliferation assay. Data are means ± SD relative to control group (n=6).

O. Immunoblots to show overexpression of HA-NRAS isoforms in hTERT/p53DD/CDK4(R24C) melanocytes.

P. hTERT/p53DD/CDK4(R24C) melanocytes were transduced with retroviruses encoding empty HA, HA-$NRAS^{WT}$, HA-$NRAS^{S89D}$, HA-$NRAS^{Q61R}$ or HA-$NRAS^{Q61R/S89D}$, and then seeded for colony formation assay. Data are means ± SD relative to control group with empty HA vector (n=6).

Q. hTERT/p53DD/CDK4(R24C) melanocytes were transduced with retroviruses encoding empty HA, HA-NRAS^{WT}, HA-NRAS^{S89D}, HA-NRAS^{Q61R} or HA-NRAS$^{Q61R/S89D}$, and then seeded for cell proliferation assay. Data are means ± SD relative to control group with empty HA vector (n=6).

R-T. Growth curve, tumor weight, and dissected tumors for the xenograft experiments with indicated cells inoculated subcutaneously into flanks of nude mice. Visible tumors were measured every three days. Data are means ± SEM relative to control group (n=7).

Figure S3. STK19 D89N is a recurrent gain-of-function mutation, related to Figure 3.

A-B. SK-MEL-2 and WM2032 cells were treated with indicated conditions, and active NRAS levels and activation of NRAS downstream signaling in the melanoma cells were detected by immunoblots.

C. SK-MEL-2 and WM2032 cells were treated with indicated conditions, and the cell proliferation rates were measured. Data are means ± SD relative to individual control group (n=6).

D. Immunoblots to show overexpression of HA-NRAS and STK19-Flag isoforms in hTERT/p53DD/CDK4(R24C) melanocytes.

E. hTERT/p53DD/CDK4(R24C) melanocytes expressing STK19 shRNA and empty HA, HA-NRAS^{WT} or HA-NRAS^{Q61R} were introduced with retroviruses encoding empty Flag, Flag-tagged STK19^{WT} or STK19^{D89N}, and then seeded for cell proliferation assay. Data are means ± SD relative to control group (n=6).

Figure S4. STK19 D89N induces melanomagenesis in the presence of oncogenic NRAS *in vivo*, related to Figure 4.

A. Schematic representation to generate the conditional knockin C57BL/6 mice with human STK19^{WT} or STK19^{D89N}.

B. PCR was performed to select mice with expression of $STK19^{WT}$ or $STK19^{D89N}$ in indicated mouse strains.

C. Immunoblots to confirm the expression of $STK19^{WT}$ or $STK19^{D89N}$ protein in indicated mouse strains.

D. Schematic representation to observe melanoma development.

E. Melanoma tissues from Tyr-Cre-$NRAS^{Q61R}$, Tyr-Cre-$NRAS^{Q61R}$-$STK19^{WT}$ and Tyr-Cre-$NRAS^{Q61R}$-$STK19^{D89N}$ knockin mice were collected for immunoblotting. Active NRAS proteins were pulled down by GST-CRAF RBD fusion protein. Active NRAS levels and activation of NRAS downstream signaling were detected by immunoblots.

Figure S5. Development of ZT-012-037-1 (1a) as a specific small molecule STK19 inhibitor, related to Figure 5.

A. Schematic representation of the *in vitro* STK19 kinase activity assay using HA-$NRAS^{Q61R}$ as the substrate.

B. The kinase assays were performed using gradient concentrations of STK19-Flag for the indicated reaction time with 100 μM ATP concentration to establish the optimal STK19 concentration (12.5 nM) and reaction time (15 min). Data are means ± SD (n = 3).

C. Gradient concentrations of ATP (0.5 μM to 200 μM) were incubated with 12.5 nM STK19-Flag for 15 min for the STK19 kinase activity assay. ATP Km (app) was calculated by fitting the data with Michaelis-Menten equation. Data are means ± SD (n = 3).

D. IC_{50} of MP-IN-317 and ZT-012-037-1 (**1a**) for inhibition of G9a enzyme activity with *in vitro* methyltransferase assay. Data are means ± SD relative to control group (n=3).

E. Relative inhibition of STK19 enzyme by ZT-012-037-1 (**1a**) and A-366 was calculated following *in vitro* kinase assay. Data are means ± SD relative to control group (n=3).

F. IC_{50} values for the inhibition of STK19 WT or mutants STK19 V134Y and L139F by **1a**. Data are means ± SD relative to control groups (n = 3).

G. Phosphorylation of HA-$NRas^{Q61R}$ was detected by immunoblots in HPMs with knockdown of STK19 and overexpression of HA-$NRas^{Q61R}$ and indicated STK19 isoforms.

H. IC_{50} values for the inhibition of $STK19^{WT}$ or $STK19^{D89N}$ by **1a**. Data are means ± SD relative to control groups (n = 3).

I. Body weight measurements of C57BL/6J mice treated with 0 or 25 mg/kg **1a** (BID) for 15 days. Data are means ± SEM relative to control groups (n = 8).

J. H&E staining of tissues in C57BL/6J mice treated with 0 or 25 mg/kg **1a** (BID) for 15 days. Scale bar, 250 μm.

Figure S6. ZT-012-037-1 (1a) inhibits oncogenic NRAS-driven melanoma development and growth, related to Figure 6.

A. Immunoblots to show overexpression of HA-NRAS and STK19-Flag isoforms in hTERT/p53DD/CDK4(R24C)-shSTK19 melanocytes.

B. hTERT/p53DD/CDK4(R24C) melanocytes infected with STK19 shRNA and retroviruses encoding empty Flag, Flag-tagged $STK19^{WT}$ or $STK19^{D89N}$ were treated with **1a** (3 μM) or not, and then seeded for cell proliferation assay. Data are means ± SD relative to control group (n=6).

C. Survival evaluation of SK-MEL-2 xenograft-bearing mice treated with **1a**. By log-rank test, $P<0.001$ (control, 25 mg/kg **1a**); $P<0.001$ (control, 50 mg/kg **1a**).

D. HPMs with depletion of STK19 and overexpression of HA-$NRAS^{Q61R}$ were transduced with retroviruses encoding empty Flag, Flag-tagged $STK19^{WT}$ or $STK19^{D89N}$, and then treated with indicated

concentrations of **1a**. Serine phosphorylation of $NRAS^{Q61R}$, active HA-NRAS levels and activation of NRAS downstream signaling were detected by immunoblots.

E. SK-MEL-2 xenograft tumors from **Figure 6G** were collected. Serine phosphorylation of $NRAS^{Q61R}$, active NRAS levels, activation of NRAS downstream signaling and H3K9 methylation were detected by immunoblots.

F. A375, UACC62, SK-MEL-2 and WM2032 cells were treated with indicated concentrations of **1a**. Serine phosphorylation of NRAS, active NRAS levels and activation of NRAS downstream signaling in these melanoma cells were detected by immunoblots.

G. A375, UACC62, SK-MEL-2 and WM2032 cells were treated with indicated concentrations of **1a** for 4 days, and the cell proliferation rates were measured. Data are means ± SD relative to individual control group (n=6).

H. A375, UACC62, SK-MEL-2 and WM2032 cells were treated with indicated concentrations of **1a** for 4 days, and the caspase activity assays were performed to investigate apoptosis. Data are means ± SD relative to individual control group (n=6).

I. SK-MEL-2 and WM2032 cells were treated with indicated low concentrations of **1a**. Serine phosphorylation of NRAS, activation of NRAS signaling and H3K9 methylation in these melanoma cells were detected by immunoblots.

J. G9a was depleted in SK-MEL-2 and WM2032 cells. Active NRAS proteins were pulled down by GST-CRAF RBD fusion protein. Active NRAS levels, activation of NRAS downstream signaling and H3K9 methylation were detected by immunoblots.

K. SK-MEL-2 cells were treated with indicated concentrations of **1a** or A-366. Serine phosphorylation of NRAS, active NRAS levels, activation of NRAS downstream signaling and H3K9 methylation were detected by immunoblots.

L. SK-MEL-2 cells were infected with retroviruses encoding empty Flag, Flag-tagged $STK19^{WT}$ or STK19 mutants, and then treated with **1a** or not. Serine phosphorylation of NRAS, active NRAS levels, activation of NRAS downstream signaling and H3K9 methylation were detected by immunoblots.

STAR★METHODS

CONTACT FOR REAGENT AND RESOURCE SHARING

Further information and requests for resources and reagents should be directed to and will be fulfilled by the Lead Contact, Rutao Cui (rutaocui@bu.edu).

EXPERIMENTAL MODEL AND SUBJECT DETAILS

Animal procedures

The generation of *Rosa26*-knock-in STK19^{WT} and STK19^{D89N} C57BL/6 mice using CRISPR/Cas9 technology was described previously (Chu et al., 2016). cDNA of human STK19^{WT} or STK19^{D89N} was inserted into the vector pR26 CAG (Addgene, #74286) via restriction enzymes AsiSI (NEB, R0630) and MluI (NEB, R3198), respectively. The generated STK19-coding construct, together with sgRosa26-1 (5'-ACTCCAGTCTTTCTAGAAGA) targeting *Rosa26* intronic XbaI site and Cas9 mRNA *in vitro* transcribed from pCAG-Cas9-162A (Addgene, #84918), were microinjected into the pronuclei of C57BL/6 zygotes. The injected zygotes were transferred into the oviducts of pseudo-pregnant NMRI female mice to obtain live pups. Microinjection and zygote injection were performed in MIT Transgenic Core. At 21 days of age, genomic DNA was extracted from the mouse tail biopsy for genotyping to examine the correct insertion of STK19^{WT} and STK19^{D89N} cDNA. The STK19 knock-in mice were further crossed with Tyr-Cre mice (purchased from Jackson Lab and originally generated by Dr. Marcus Bosenberg (Dankort et al., 2009)) and loxP/STOP/loxP NRAS^{Q61R} knockin (LSL-NRAS^{Q61R}) mice (kind gifts from Drs. Norman Sharpless and David Fisher) to generate indicated mice for experiments. All mice were maintained in a specific-pathogen-free facility of the Animal Science Center (ASC) of Boston University Medical Campus, and the experiments were performed according to the Institutional Animal Care and Use Committee of Boston University Medical Campus. Mice were housed on a time cycle of 12 h of light (beginning at 6:00) and 12 h of dark (beginning at 18:00). Mice were allowed free access to an irradiated diet and sterilized water. The mice were monitored daily for signs of health status and distress.

For the toxicity profile of **1a** inhibitor in C57BL/6J mice, vehicle [5% (w/v) Kolliphor HS 15 (Sigma)] in normal saline or 25 mg/kg of **1a** formulated in the vehicle was injected twice a day (BID). Mouse body weights were measured every day. After indicated days, mice were euthanized. The serum was acquired for blood biochemistry analyses using assay kits according to manufacturer's instructions (Shenzhen Mindray Bio-Medical Electronics Co., Ltd.). The organs were separated and processed for H&E staining. Specifically, tissues were fixed in 4% paraformaldehyde and embedded in paraffin. Then, 4 μm thick slices were stained with haematoxylin and eosin and examined by light microscopy (Leica DM4 M).

For *in vivo* tumorigenesis assay, 2×10^6 hTERT/p53DD/CDK4(R24C) melanocytes or SK-MEL-2 melanoma cells mixed with matrigel (1:1) were injected subcutaneously into the flanks of 8-week female nude mice. Tumor size was measured every 3 days with a caliper, and the tumor volume was determined with the formula: Length × Width^2 × 0.5. To investigate the inhibitory effects of ZT-12-037-1 (**1a**) on melanomagenesis, 25 mg/kg **1a** was intraperitoneally injected once a day. For SK-MEL-2 tumors, 25 mg/kg **1a** was intraperitoneally injected once or twice a day (25 or 50 mg/kg/day) after the tumors have grown to 100-200 mm^3. The mice were euthanized after indicated days or when the allowable endpoint size (1 cm^3) was reached. None of the xenograft tumors reached the maximal tumor volume permitted by the IACUC of Boston University Medical Campus. The xenograft tumors were dissected and their weights were measured.

Primary melanocytes and cell culture

Human primary melanocytes (HPMs) were isolated from normal discarded foreskins as described before (Chen et al., 2017) and were cultured in Medium 254 (Thermo Fisher Scientific) supplemented with Human Melanocyte Growth Supplement (HMGS, Thermo Fisher Scientific, S-002-5). Immortal human melanocytes (hTERT/p53DD/CDK4(R24C)) (Garraway et al., 2005) were cultured in glutamine containing Ham's F12 media supplemented with 7% fetal bovine serum (FBS), 0.1 mM IBMX, 50 ng/mL

TPA, 1 μM Na_3VO_4, and 1 μM dibutyryl cAMP. All melanoma cell lines are mycoplasma-negative and maintained in Dulbecco's Modified Eagle's Medium (DMEM) containing 10% fetal bovine serum (FBS), 100 units of penicillin and 100 mg/mL streptomycin.

METHOD DETAILS

Plasmids and shRNAs

The Flag-tagged wild-type STK19 encoding plasmid was purchased from Origene (RC219373L3). The HA-tagged wild-type NRAS encoding plasmid pCGN NRAS wt was purchased from Addgene (14723). To generate the STK19 or NRAS expression plasmids for retroviral infection, the cDNA were subcloned into pQCXIP (Clonetech) at the NotI/EcoRI sites, respectively. All other mutants were generated by site-directed mutagenesis using QuikChange II Site-Directed Mutagenesis Kit (Agilent) according to the manufacture's instruction. To overexpress wild-type STK19 or NRAS and their mutants, HEK293FT cells were co-transfected with pQCXIP-STK19 or pQCXIP-NRAS, pCMV-VSV-G (Addgene, 8454) and pUMVC (Addgene, 8449) using Lipofectamine 3000 (Thermal Fisher Scientific) as described previously (Chen et al., 2017). Retroviruses were collected 48 h after the transfection, and infected cells for 24 h in the presence of 8 μg/mL polybrene. The infected cells were then selected by 2 μg/mL puromycine. To knockdown STK19 in melanocytes and melanoma cells, human specific short hairpin RNAs in pLKO.1 targeting STK19 were co-transfected with psPAX2 (Addgene, 12260) and pMD2.G (Addgene, 12259) into HEK293FT cells using Lipofectamine 3000. Lentiviruses were harvested 48 h after the transfection, and infected cells for 24 h in the presence of 8 μg/mL polybrene. The infected cells were then selected by 2 μg/mL puromycine.

High-throughput siRNA screening of NRAS regulators

The *Silencer*™ Human Kinase siRNA Library (Thermo Fisher Scientific) contains 2,127 siRNA targeting 709 human kinase genes (3 siRNA pooled per gene) supplied in 96-well plates. HEK293FT cells infected with recombinant lentiviruses encoding HA-tagged $NRAS^{Q61R}$ were transfected with each kinase siRNA from the library (final concentration at 20 nM) using Lipofectamine 3000 (Thermo Fisher Scientific) according to the manufacturer's instructions. At 48 h after transfection, whole cell lysates from HEK293FT cells were collected for RAS activity assay using modified RAS GTPase ELISA Kit (Abcam). Specifically, active RAS proteins were captured by GST-CRAF-RBD fusion protein in glutathione-coated plates. The bound HA-$NRAS^{Q61R}$ was incubated with a horseradish peroxidase (HRP)-conjugated antibody against HA tag (Abcam) at room temperature for 30 min. The Pierce™ ECL Western Blotting Substrate (Thermo Fisher Scientific) was added to generate a sensitive chemiluminescence readout. The levels of RBD-bound HA-$NRAS^{Q61R}$ after silencing each kinase individually were quantified in relation to control siRNA.

Quantitative real-time PCR (qRT-PCR)

Total RNA was extracted with Qiagen RNeasy kit (Invitrogen). cDNA was synthesized using SuperScript II Reverse Transcriptase (Invitrogen), and 40 ng cDNA was used for quantitative real-time PCR amplification with TaqMan™ Gene Expression Master Mix (Thermo Fisher Scientific). The relative levels of STK19 expression were normalized according to those of GAPDH. qRT-PCR data were calculated using the comparative C_T method. All quantitative PCR were performed in triplicates.

Immunoblot analysis

Whole cell lysates were prepared using lysis buffer containing 50 mM Tris pH 7.4, 1% Triton X-100, 0.5 mM EDTA, 0.5 mM EGTA, 150 mM NaCl, 10% glycerol, 1 mM phenylmethylsulfonyl fluoride and complete protease inhibitor cocktail (Roche), homogenized and centrifuged at 14,000 rpm for 15 min at 4 °C. Protein concentration of cell lysates was determined by Pierce BCA Protein Assay Kit (Thermo Fisher Scientific). Cell lysates were incubated in Pierce™ Lane Marker Reducing Sample Buffer for 5

min at 100 °C, separated by 8-12% SDS-PAGE, transferred to PVDF membrane (BIO-RAD) and probed with specific primary and horseradish peroxidase (HRP)-conjugated antibodies. Pierce™ ECL Western Blotting Substrate (Thermo Fisher Scientific) was used for detection of protein of interest.

Co-immunoprecipitation

In brief, cells were washed three times with ice-cold phosphate-buffered saline (PBS) and lysed in lysis buffer containing 50 mM Tris pH 7.4, 1% Triton X-100, 0.5 mM EDTA, 0.5 mM EGTA, 150 mM NaCl, 10% Glycerol, 1 mM phenylmethylsulfonyl fluoride and complete protease inhibitor cocktail (Roche) on ice for 30 min. The cell lysates were centrifuged at 15,000 × g for 15 min at 4 °C and 500 μg supernatant was precleared by Protein G Agarose Beads (Thermo Fisher Scientific) and incubated with different primary antibodies overnight at 4 °C, or incubated with Flag/HA beads (Sigma-Aldrich) directly for 2 h at room temperature. Protein G Agarose Beads were added into cell lysates for incubation with rotation at 4 °C for 1 h. After three washes with 1 mL of lysis buffer, the bound proteins were resolved by SDS-PAGE and immunoblotted with indicated antibodies.

RAS-GTP Pull-down

Active RAS-GTP levels were assessed by Active RAS Pull-Down and Detection Kit (Thermo Fisher Scientific) according to the manufacture's instruction. Specifically, 500 μg whole cell lysates were incubated with 30 μL glutathione resin and GST-RBD fusion protein for 1 h at 4 °C to capture active RAS-GTP proteins. The GST-RBD-bound RAS proteins were recovered by washing and elution. The purified NRAS proteins and HA-NRAS recombinant proteins were detected by immunoblot analysis using the primary antibodies targeting NRAS (Abcam) and HA tag (Abcam).

***In vitro* kinase assay**

Recombinant HA-NRAS proteins were preloaded with GDP, GTP, or GTPγS and subjected to the *in vitro* kinase assay with purified recombinant STK19-Flag proteins in kinase buffer containing 20 mM $MnCl_2$, 50 mM HEPES (pH 8.0) supplemented with 300 μM AMP and 100 μM ATP (or ATP mixture with γ-^{32}P-ATP) for 30 min at 30 °C. The phosphorylated HA-NRAS was pulled down by anti-HA beads and proceeded for SDS-PAGE. Phosphorylation of NRAS was detected by subsequent immunoblotting and autoradiography.

Mass spectrometry

Liquid chromatography/tandem mass spectrometry was performed by Taplin Biological Mass Spectrometry Facility, Harvard Medical School. For identification of STK19-interacting proteins, cell lysates of SK-MEL-2 overexpressing human recombinant Flag-tagged STK19 were isolated by anti-Flag magnetic agarose beads. For identification of phosphorylated amino acids in NRAS by STK19, HA-NRAS protein was pulled down by anti-HA magnetic agarose beads after *in vitro* kinase reaction with STK19-Flag. The prepared protein samples were incubated with sample buffer for 5 min at 100 °C, and then separated by SDS-PAGE. The gel was immersed in staining solution (0.3% Coomassie blue, 45% methanol, 10% glacial acetic acid and 45% dH2O) on shaker for 30 min, followed by incubation in destaining solution (20% methanol, 10% glacial acetic acid, and 70% dH_2O) on the shaker overnight. The bands were excised and sent to Taplin Biological Mass Spectrometry Facility in Harvard Medical School for protein identification and protein phosphorylation identification.

Colony formation and cell proliferation assays

The colony formation assay for hTERT/p53DD/CDK4(R24C) melanocytes were performed as described before. Briefly, hTERT/p53DD/CDK4(R24C) melanocytes infected with indicated plasmids were plated into 6-well plate at 2,500 cells per well and cultured for 14 days. The colonies were fixed with 10% (v/v) methanol for 15 min and stained with 5% Giemsa (Sigma) for 30 min for colony visualization. Cell

proliferation rates were determined by CyQUANT™ NF Cell Proliferation Assay Kit (Invitrogen) according to the manufacturer's protocol. In brief, cells were plated at density of 100-500 cells per well in a 96-well microplate. After indicated treatment for 4 days, CyQUANT® NF dye solution was added to each well to generate fluorescence readout after binding with DNA. The fluorescence intensity was measured using a fluorescence microplate reader with 485/520 nm filter set. The relative cell number stands for fold change in relation to the cell number of control group.

Melanin staining

The melanin staining in mouse ears was performed with the Fontana-Masson kit (Abcam, ab150669) following the manufacturer's protocol. Briefly, the sectioned ear tissues were hydrated and incubated successively in warmed ammoniacal silver solution for 30 min, gold chloride solution (0.2%) at room temperature for 30 s, sodium thiosulfate solution (5%) at room temperature for 1 min, and nuclear fast red solution for 5 min. After dehydration, the slide was mounted and observed with an Olympus Inverted microscope (Cellular imaging core, Boston University).

Optimization and validation of the STK19 kinase assay

The optimal conditions of the STK19 enzyme and the ATP concentrations in the 96-well format kinase assay were first determined using Promega ADP-Glo® kinase assay according to the manufacture's protocol. For the enzyme concentration and reaction time optimization, Flag-tagged STK19 at various concentrations (ranging from 0.2 to 400 nM), ATP (100 μM) and the substrate HA-tagged GTP-preloaded NRAS (1 μM) were added to 96-well white solid plates (15 μL volume) for 0 to 40 min in the kinase buffer. The kinase reaction was stopped by ADP-Glo™ Reagent and the ADP generated in the kinase reaction was converted to ATP for luciferase assay. Phosphorylation of HA-tagged NRAS was quantified based on the luminescence readout measured with Tecan Infinite® M1000 Microplate Reader. The optimal amount of STK19 is the minimal amount that produces luminescence within the linear portion of

the kinase titration curve and generates an adequate signal-to-background ratio. The optimal kinase reaction time was defined as the point at which the EC_{50} from the enzyme titration no longer changes. We finally chose 12.5 nM STK19 and 15 min as the optimal kinase concentration and reaction time for the kinase assay. The ATP titration was conducted with STK19 kinase using the enzyme concentration previously determined, and the kinase assays were performed at ATP concentrations ranging from 0.5 μM to 200 μM. The apparent ATP Km(app) was calculated by fitting data using the Michaelis-Menten equation. The ATP concentration of 6.36 μM Km(app) for STK19 was determined to show a 50% change between the maximum and minimum phosphorylated NRAS levels.

Assay quality was determined using the Z-factor, indicating the quality of an assay. Z-factors of 0.5 or greater indicate an excellent assay. The assay optimization procedure uses the wells in the row that contain no kinase as the 100% inhibition control wells and each of the wells in the row containing STK19 as the 0% inhibition control wells. The Z-factor value was calculated using the following equation:

$$\text{Z-factor} = 1 - 3 \times (\sigma_{0\%\text{Inhibition}} + \sigma_{100\%\text{Inhibition}}) / (\mu_{0\%\text{Inhibition}} - \mu_{100\%\text{Inhibition}}),$$

where σ represents standard deviation and μ represents the mean value of the luminescence. The Z-factor was 0.703 for Flag-tagged STK19, confirming the optimization of the enzyme concentration, the reaction time and the ATP concentration.

Procedures for chemical synthesis of ZT-12-037-01 (1a)

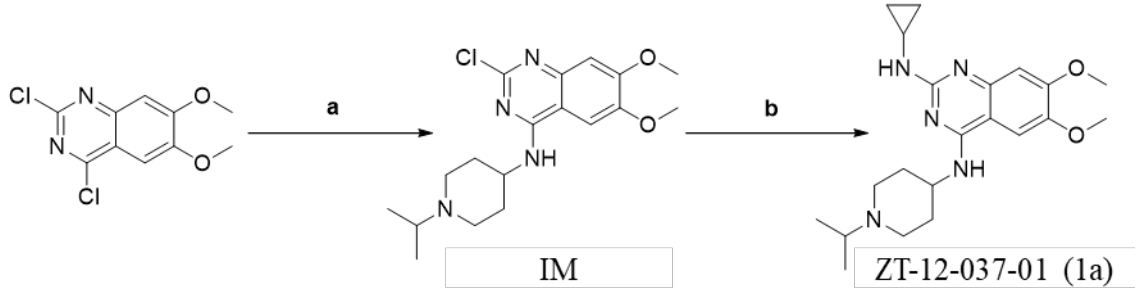

Reagents and conditions: a) 1-isopropylpiperidin-4-amine, DMF, K_2CO_3, room temperature, 6 h; b) cyclopropanamine, TFA, MW, 110 ℃, 1 h.

2-chloro-N-(1-isopropylpiperidin-4-yl)-6,7-dime thoxyquinazolin-4-amine (IM)

To a stirred solution of 2,4-dichloro-6,7-dimethoxyquinazoline (259.1 mg, 1 mmol) in DMF (5 mL) was added K_2CO_3 (207.03 mg, 1.5 mmol) and 1-isopropylpiperidin-4-amine (170.7 mg, 1.2 mmol). After stirring for 6 h, the reaction was quenched with water and extracted with EtOAc (3 × 20 mL). The combined organic layers were dried over anhydrous Na_2SO_4, filtered, and concentrated under reduced pressure. The crude solid was purified by silica gel chromatography [MeOH (1.75 N NH_3)/CH_2Cl_2 = 1: 10] to afford compound **1** as white crystals (300 mg, 82.2% yield). ^{1}H NMR (600 MHz, $CDCl_3$) δ 7.13 (s, 1H), 6.77 (s, 1H), 4.34 – 4.18 (m, 1H), 4.01 (s, 3H), 3.98 (s, 3H), 2.94 – 2.88 (m, 2H), 2.79 (p, *J* = 6.5 Hz, 1H), 2.46 – 2.32 (m, 2H), 2.22 – 2.13 (m, 2H), 1.64 – 1.56 (m, 2H), 1.08 (d, *J* = 6.6 Hz, 6H). MS (ESI) *m/z*: 365$[M+H]^+$.

N^2-cyclopropyl-N^4-(1-isopropylpiperidin-4-yl)-6,7-dimethoxyquinazoline-2,4-diamine (ZT-12-037-01, 1a)

The intermediate IM (36.5 mg, 0.1 mmol) was dissolved in cyclopropanamine (0.5 mL) and treated with trifluoroacetic acid (74.3 uL, 1 mmol). The solution was heated in microwave synthesizer (Initiator™) at 110 °C for 1 h, then it was concentrated under reduced pressure. The resulting residue was purified by preparative HPLC to yield the creamy white compound (31.3 mg, 81.2%). ^{1}H NMR (600 MHz, $CDCl_3$) δ 7.28 (s, 1H), 6.85 (s, 1H), 4.49 – 4.32 (m, 1H), 3.97 (s, 3H), 3.93 (s, 3H), 3.40 – 3.28 (m, 2H), 3.29 – 3.17 (m, 1H), 2.85 – 2.74 (m, 1H), 2.78 – 2.64 (m, 2H), 2.35 – 2.27 (m, 2H), 2.28 – 2.14 (m, 2H), 1.31 – 1.23 (m, 6H), 0.81 – 0.70 (m, 2H), 0.72 – 0.61 (m, 2H). ^{13}C NMR (150 MHz, $CDCl_3$) δ 159.3, 156.2, 155.0, 147.3, 117.9, 116.0, 103.2, 102.3, 56.8, 56.7, 56.7, 47.8, 29.3, 23.9, 17.5, 6.8. MS (ESI) *m/z*: 386$[M+H]^+$. HRMS (ESI) calculated for $C_{21}H_{32}N_5O_2$ $[M+H]^+$, 386.2556; found, 386.2551.

Differential scanning fluorimetry (DSF) assay

The thermal denaturation of STK19-Flag was determined by DSF assay using Protein Thermal Shift™ Dye Kit (Thermal Fisher Scientific). In brief, the purified recombinant protein was diluted to a final concentration of 10 μM in 100 mM Tris buffer (pH 8.0). **1a** (final concentration at 100 μM) was added to obtain 20 μL of assay volume. Heat gradient from 25 °C (100%) to 99 °C (1%) was conducted in QuantStudio 12K Flex Real-Time PCR System. The melt curve was recorded and the melting temperature was determined using the inflection points of the plots of d(RFU)/dT.

***In vivo* proliferation and apoptosis assay**

The xenograft tumor tissues were isolated and mounted in O.C.T. embedding compound (Fisher Healthcare) and cut into 8 μm sections (Dermpath core facility, Boston University). For immunostaining, after thawing and rehydration, the slides were blocked with 0.1% Tween-20 and 5% normal goat serum (Jackson ImmunoResearch) in PBS for 1 h at room temperature for nonspecific staining, and incubated with primary antibodies against Ki67 and cleaved caspase 3 overnight at 4 °C. Then, slides were incubated with fluorescent-labelled corresponding secondary antibodies for 1 h at room temperature. The slides were mounted with ProLong Gold Antifade Mountant with DAPI (Thermo Fisher Scientific). Images were taken with a laser scanning confocal microscope Leica SP5 (Cellular imaging core, Boston University).

QUANTIFICATION AND STATISTICAL ANALYSIS

All quantitative data were presented as the mean ± SD or SEM of at least three independent experiments by Student's paired or unpaired two-tailed t-test or two-way ANOVA, as appropriate. (*P < 0.05, **P < 0.01, ***P < 0.001, n.s., not significant). For survival analysis, the Kaplan–Meier survival curves were compared using the log–rank test. Analyses were performed using GraphPad Prism V7.

Figure 1

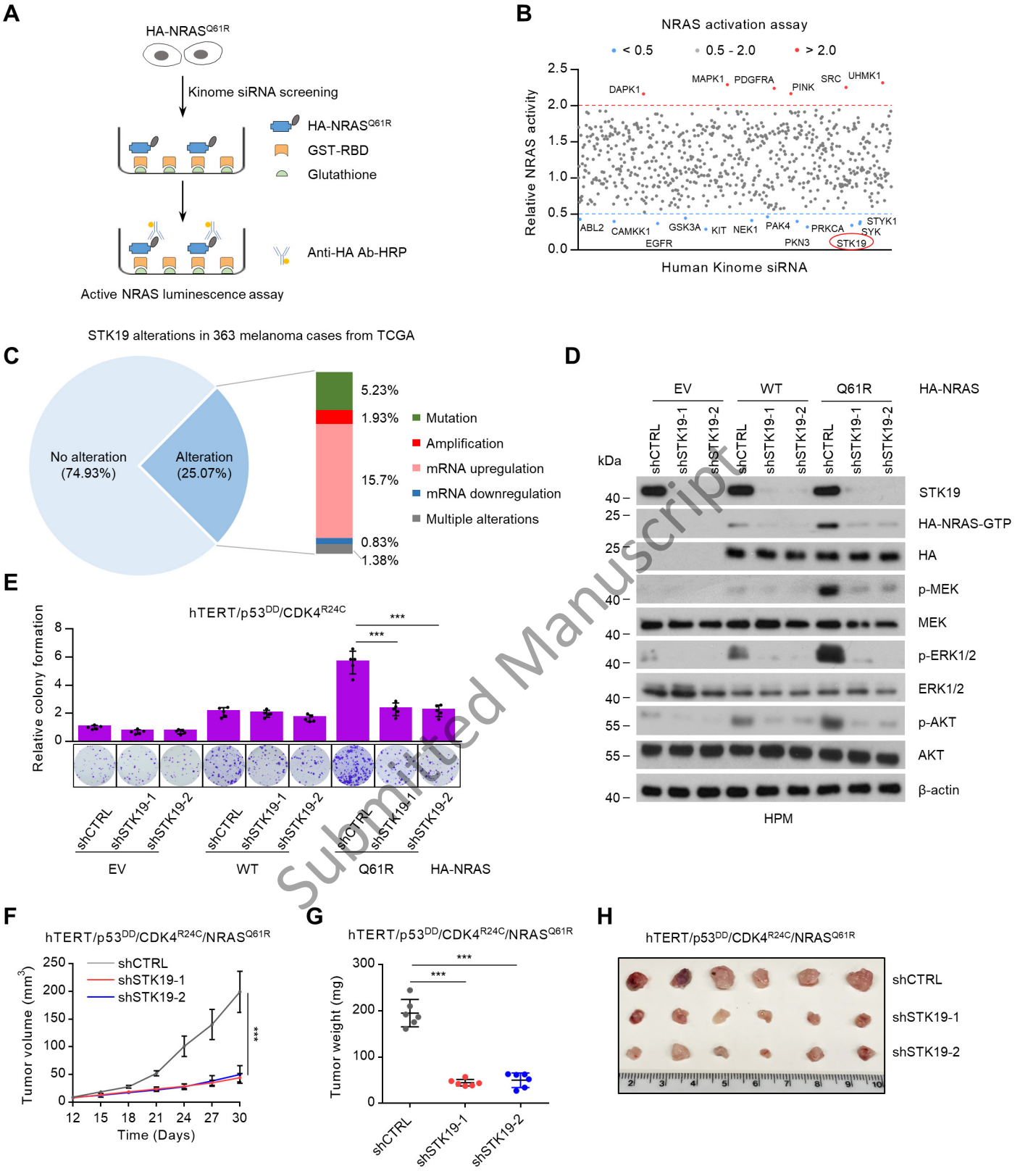

Figure 2

A

Mass spectral peptide count

Protein	Unique
STK19	25
NRAS	13
YWHAE	8
PABPC1	8
ENO1	5
PHB2	4
PSMC5	3
ILF2	3
UBAP2L	3
HNRNPM	3

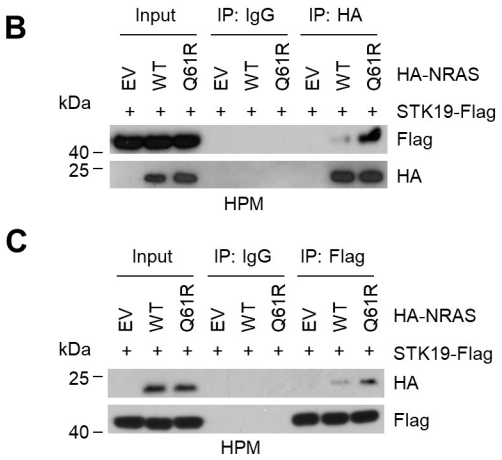

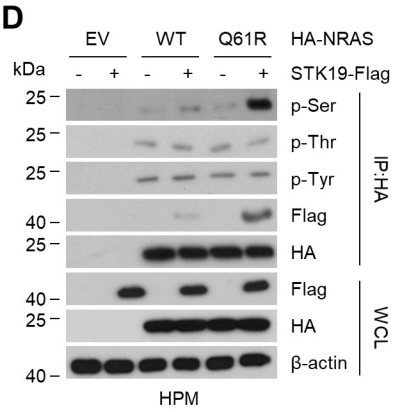

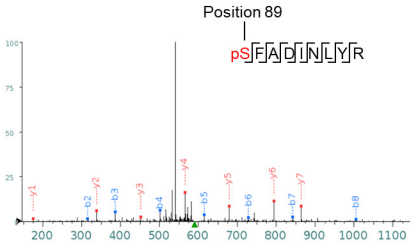

F

```
NRAS_HUMAN    81 VFAINNSKSFADINLYREQI 100
NRAS_MOUSE    81 VFAINNSKSFADINLYREQI 100
NRAS_RAT      81 VFAINNSKSFADINLYREQI 100
NRAS_CAVPO    81 VFAINNSKSFADINLYREQI 100
NRAS_XENLA    81 VFAINNSKSFADINAYREQI 100
                        89
```

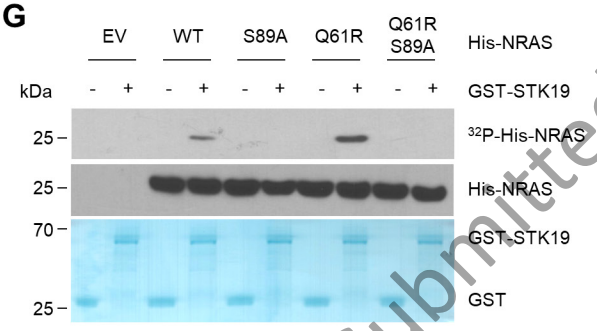

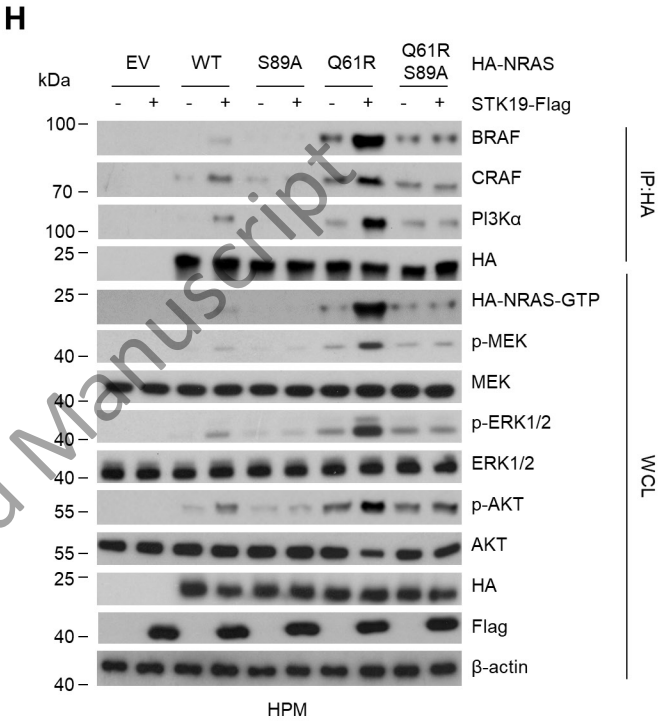

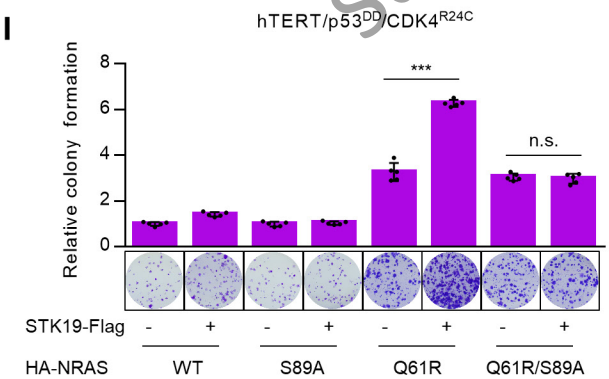

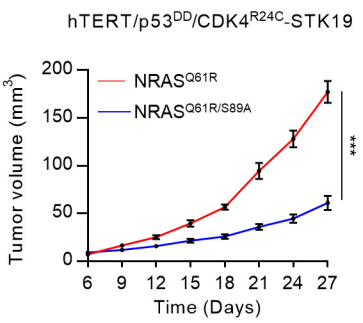

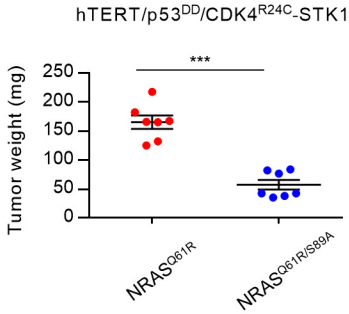

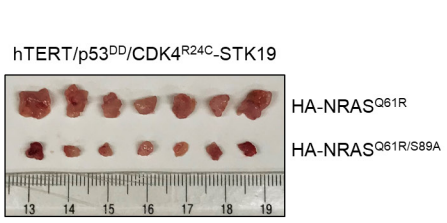

Figure 3

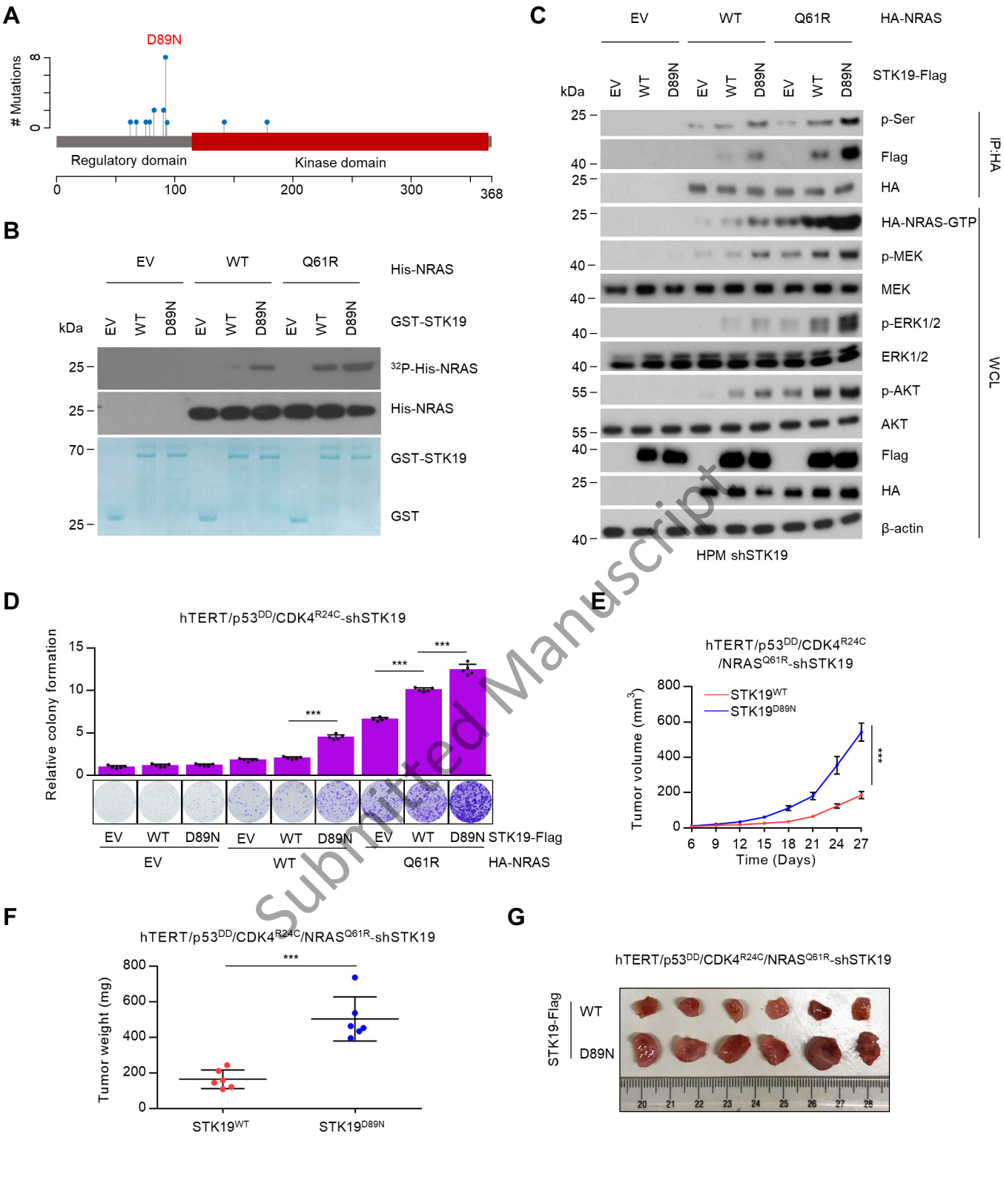

Figure 4

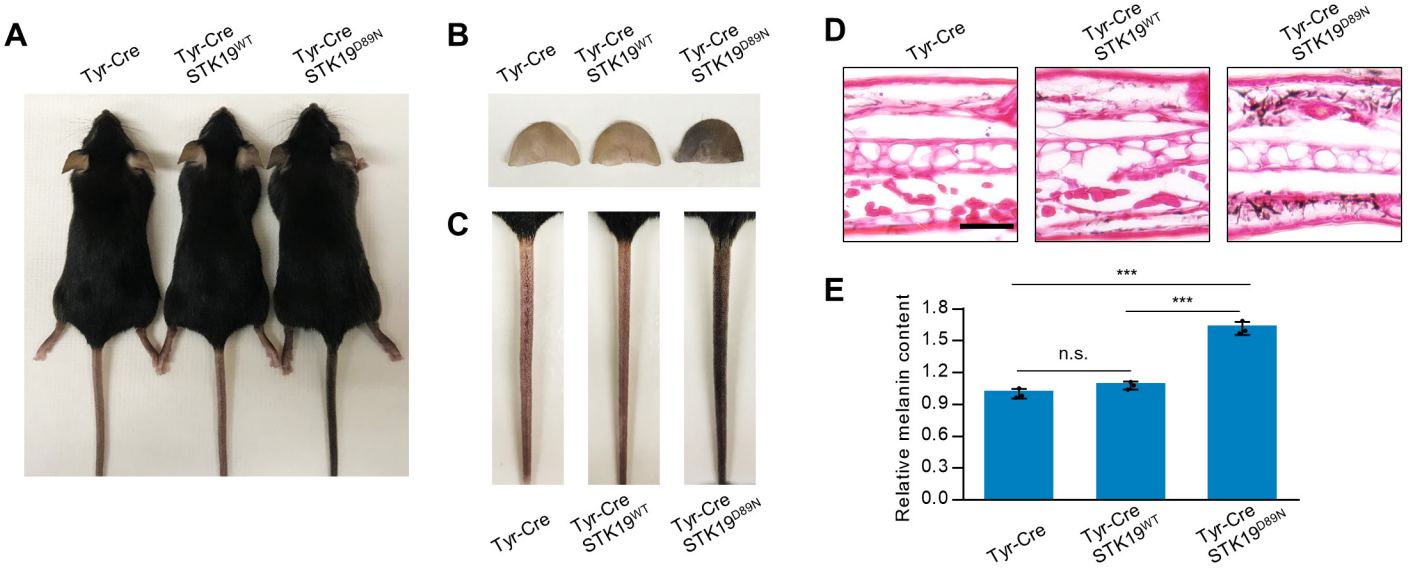

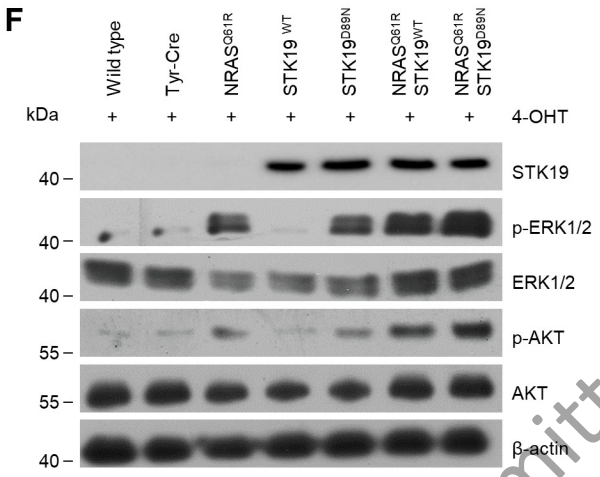

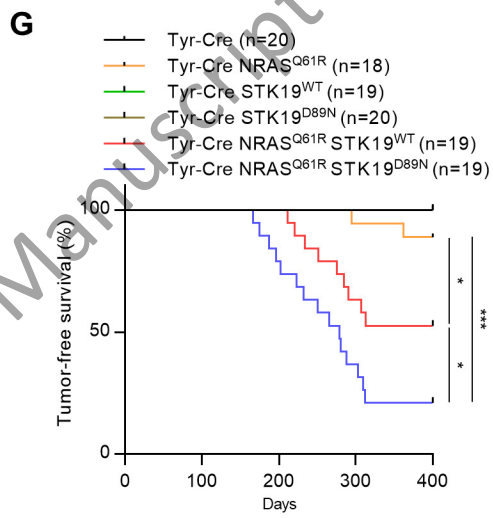

Figure 5

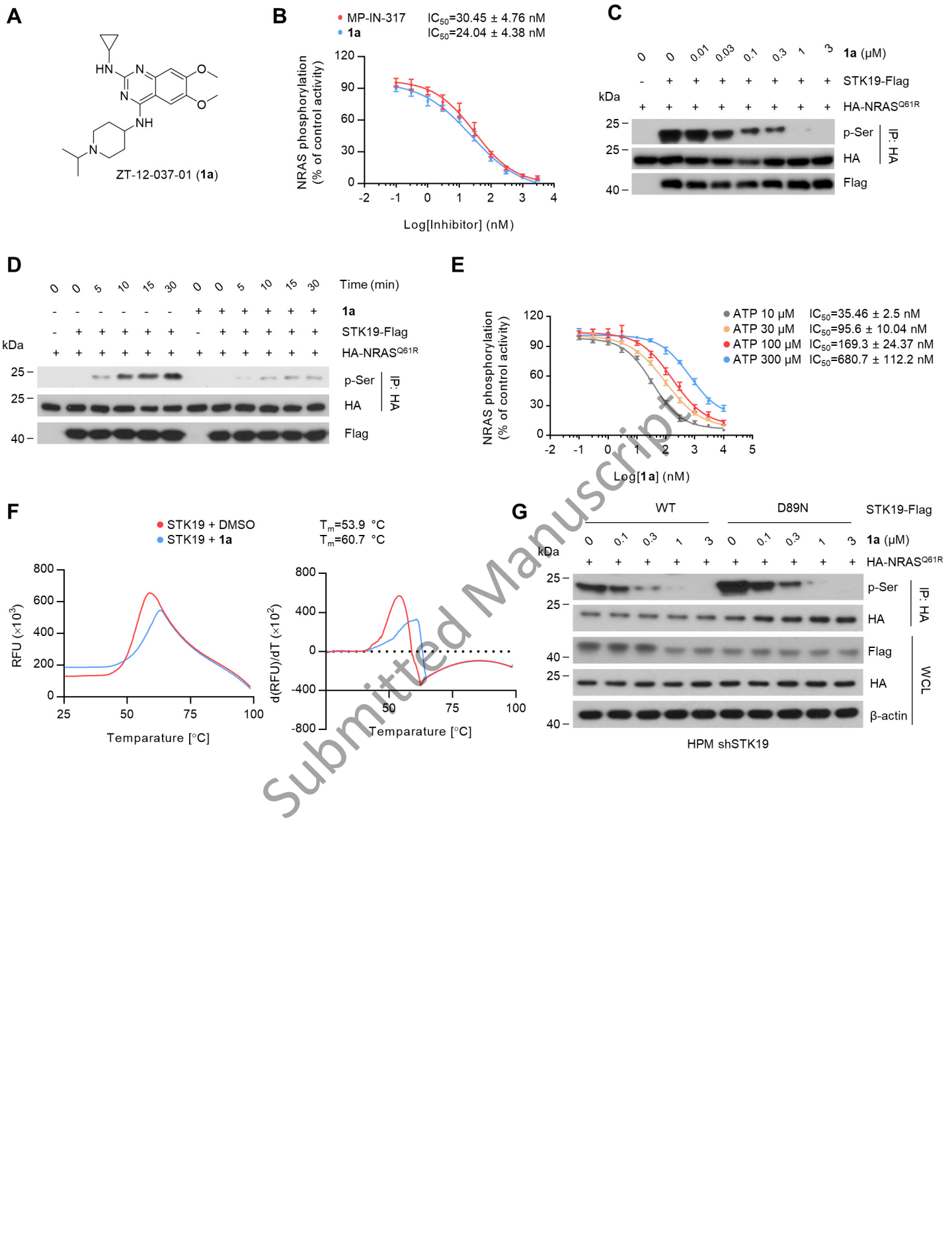

Figure 6

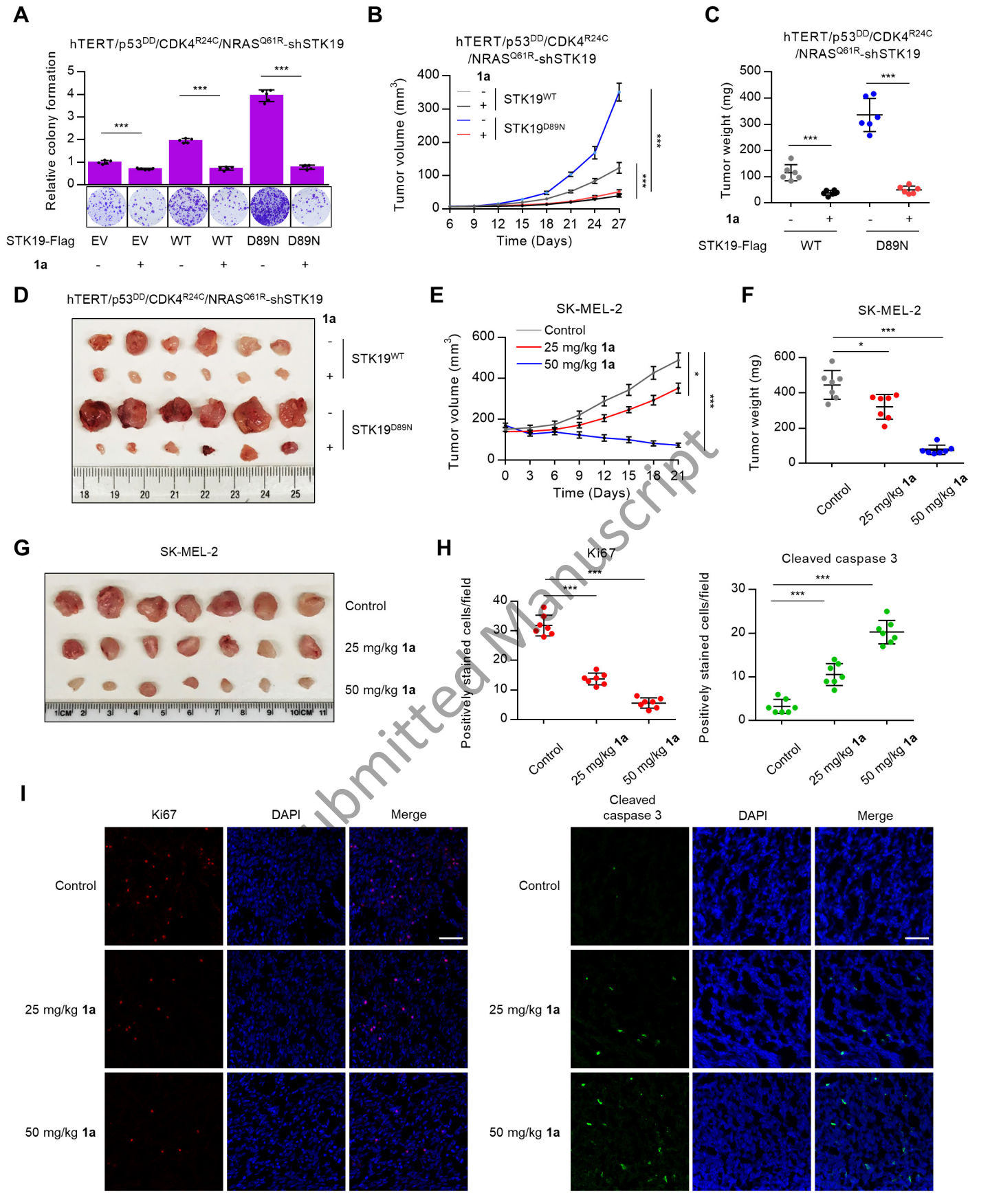

Figure S1

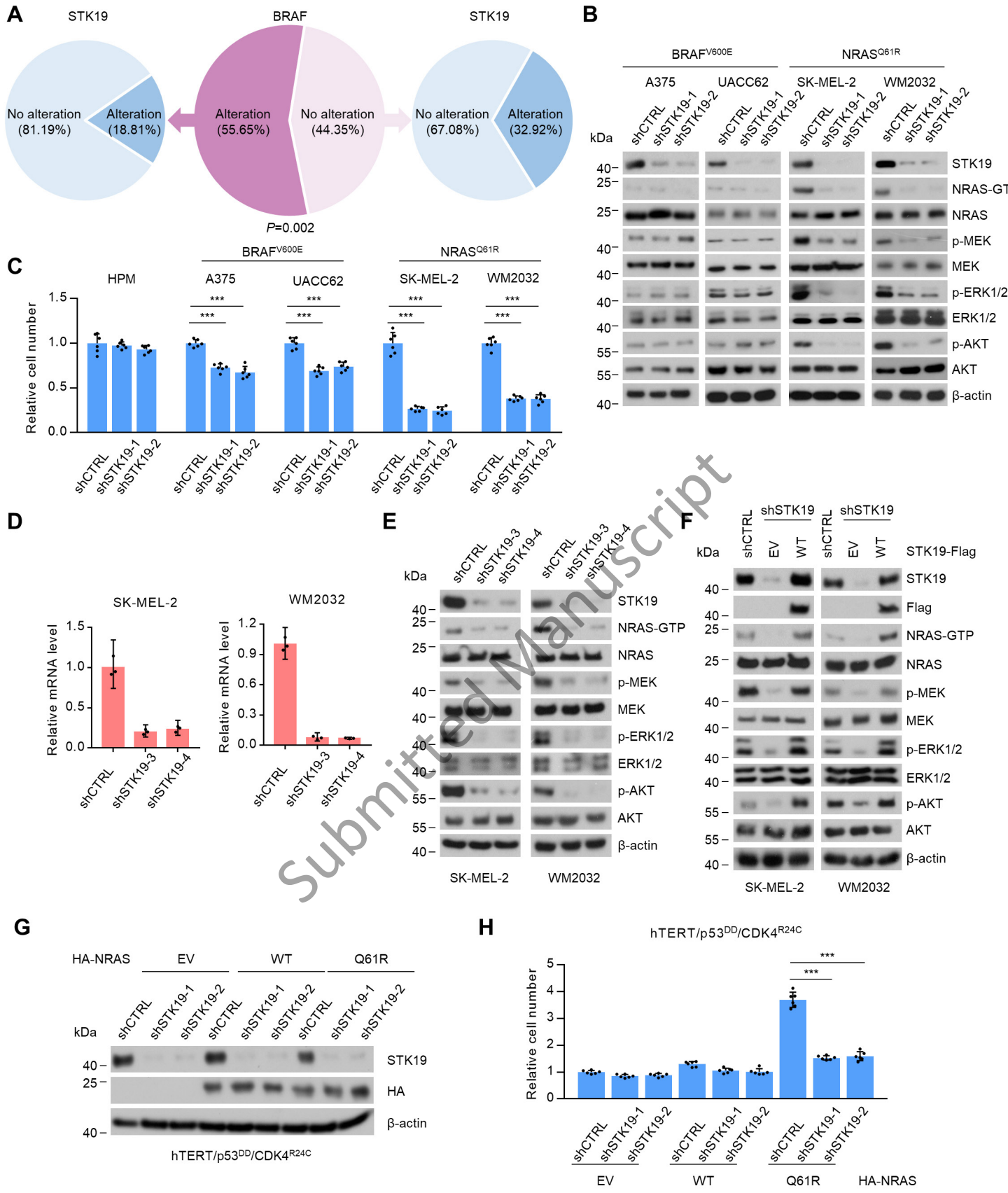

Figure S2

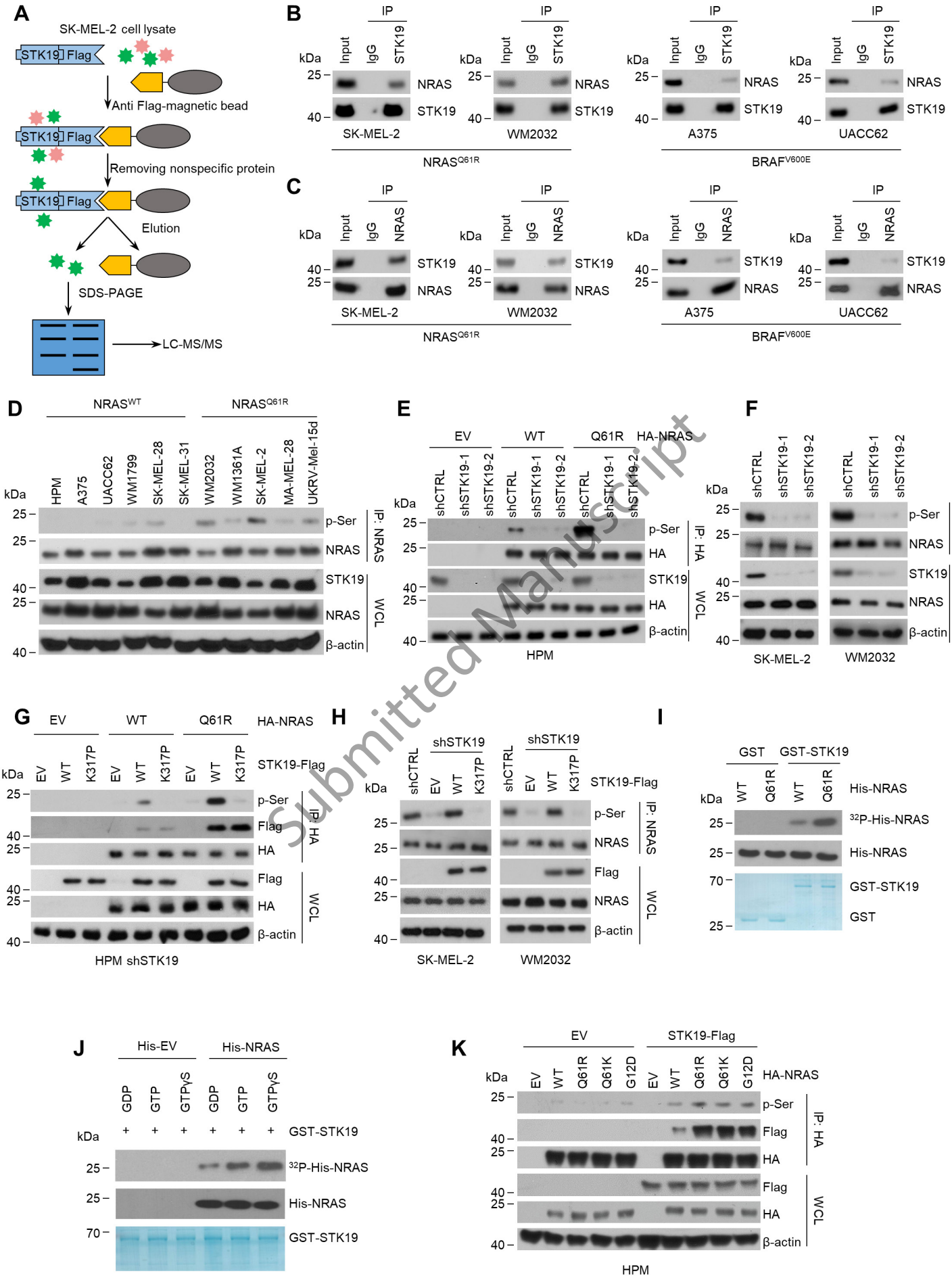

Figure S2

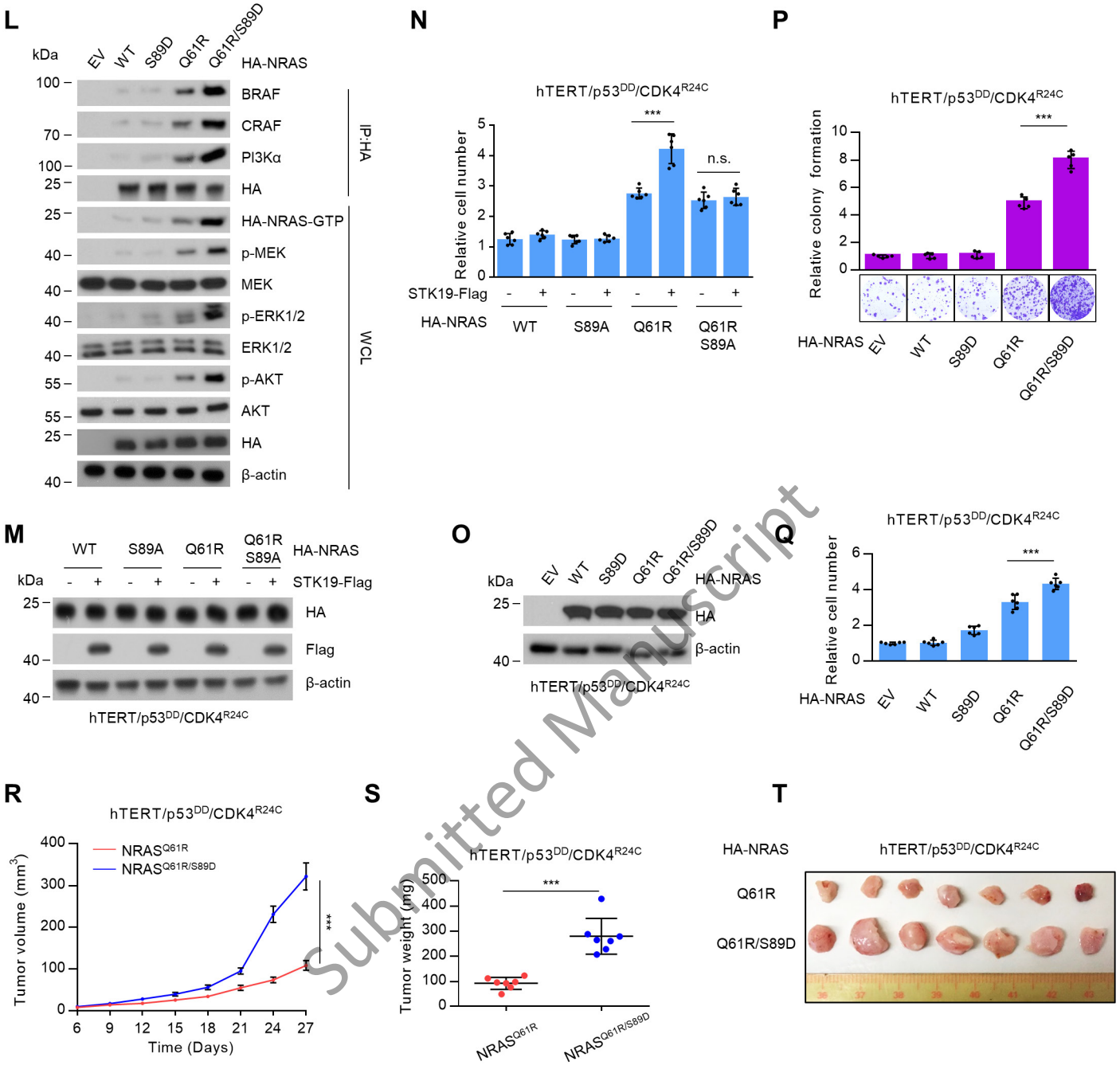

Figure S3

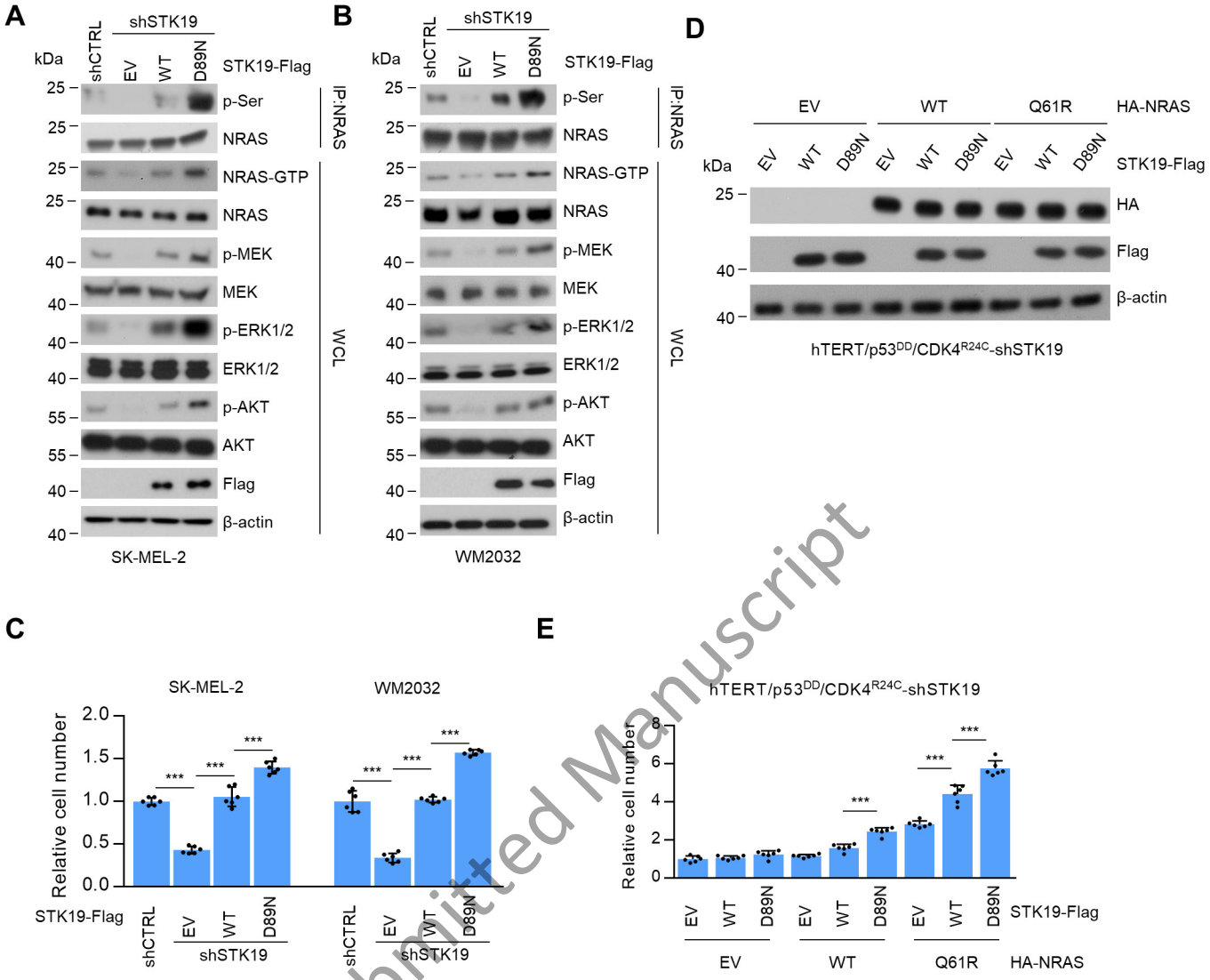

Figure S4

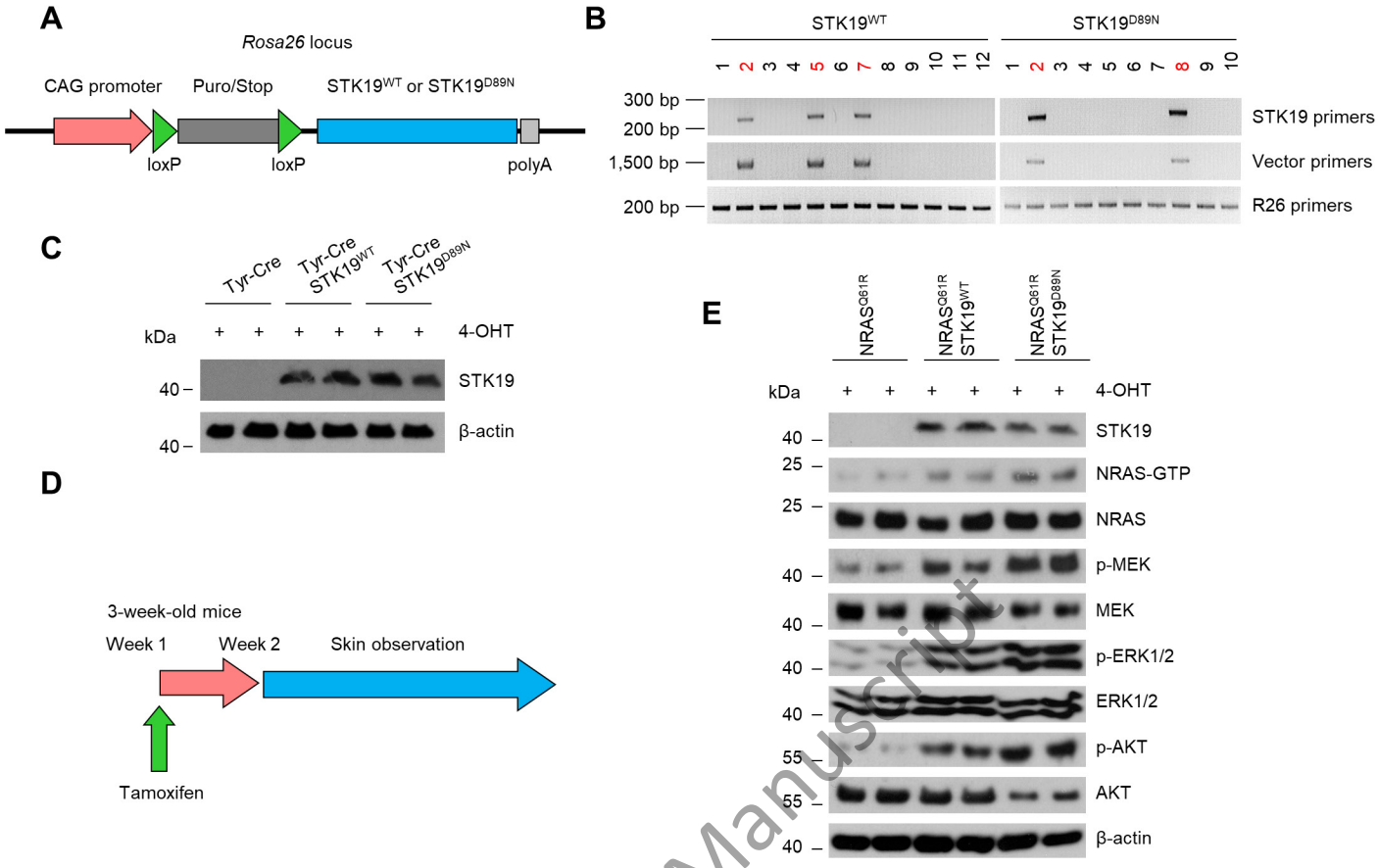

Figure S5

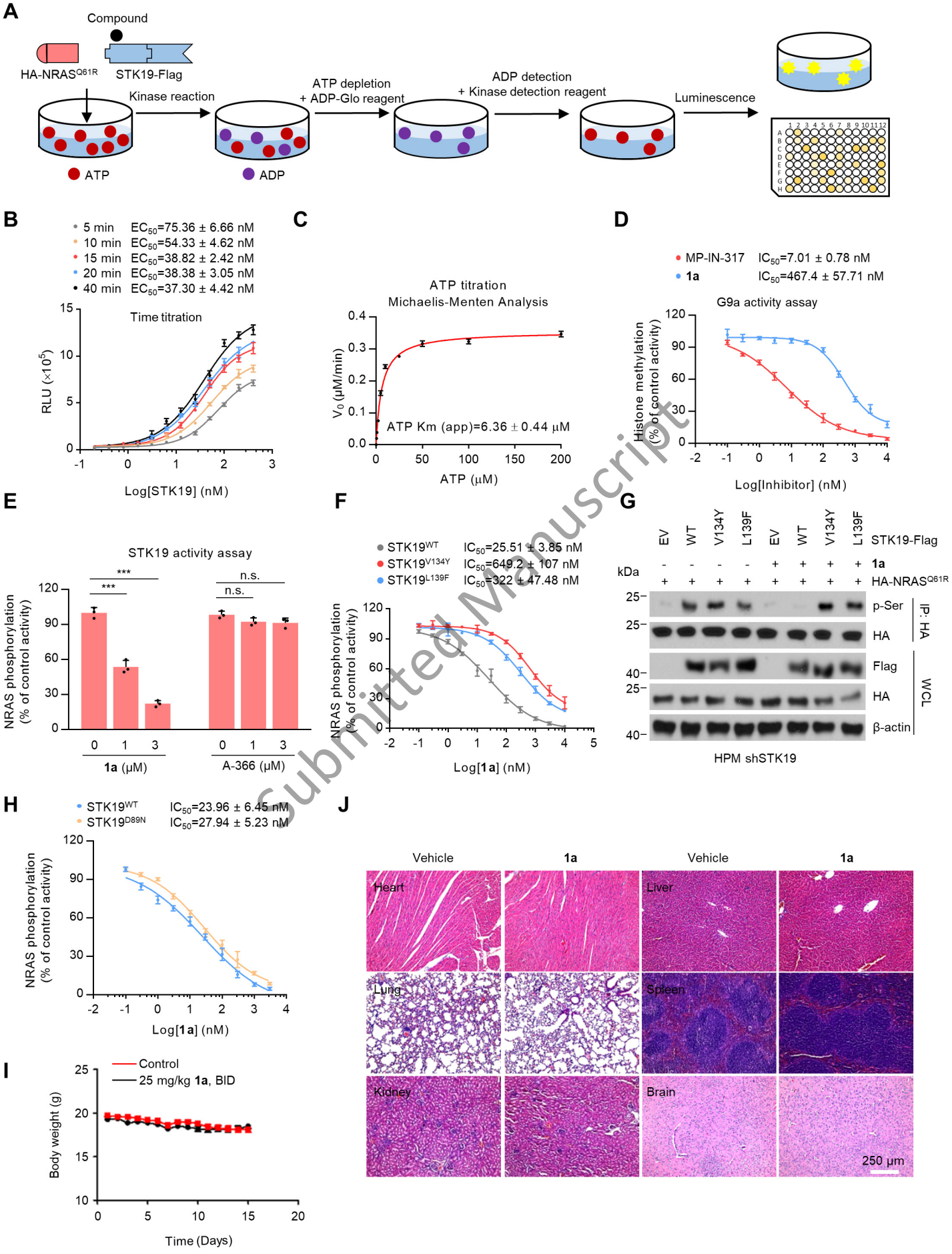

Figure S6

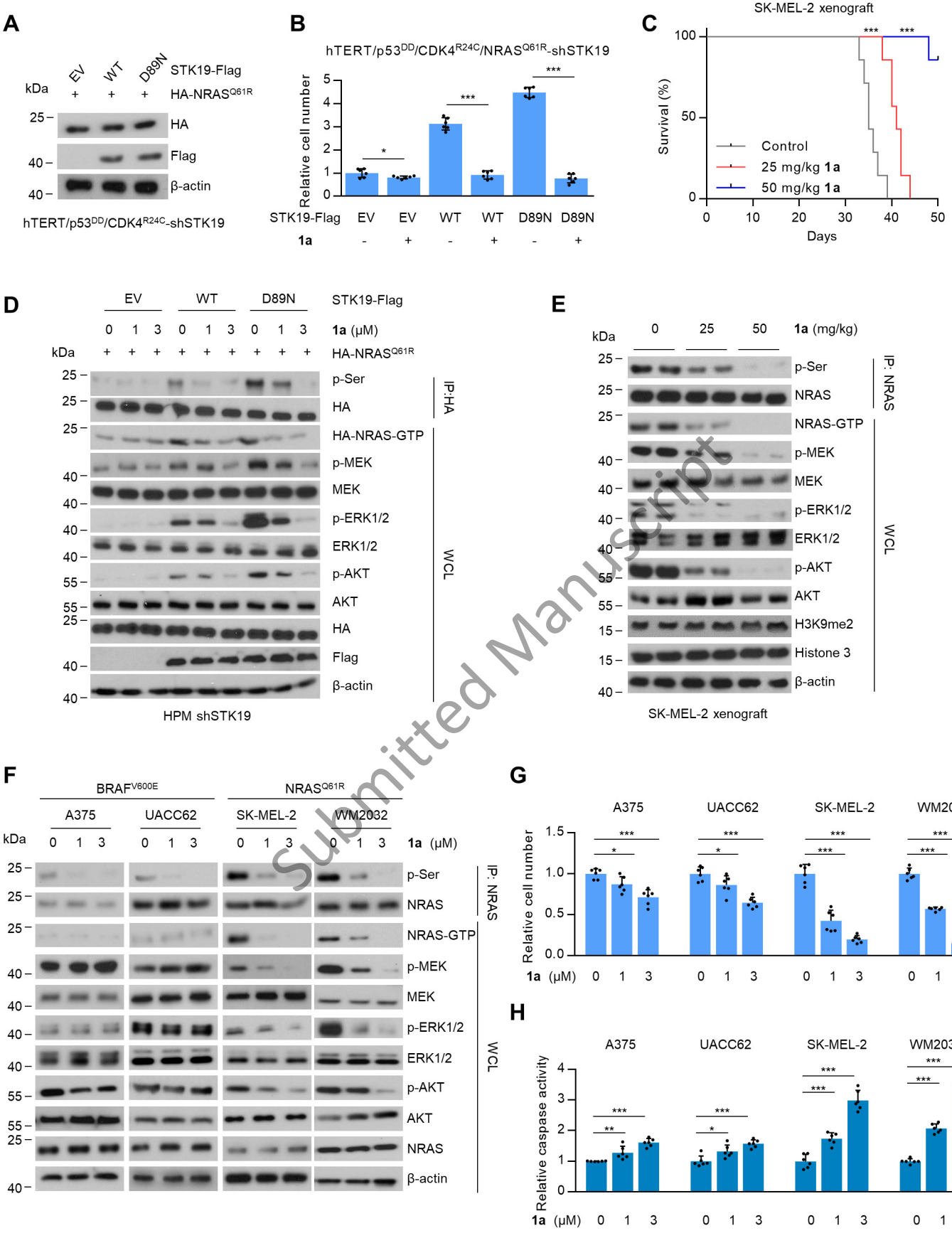

Figure S6